Published OnlineFirst August 2, 2021; DOI: 10.1158/2326-6066.CIR-21-0062

Bispecific CAR T Cells against EpCAM and Inducible ICAM-1 Overcome Antigen Heterogeneity and Generate Superior Antitumor Responses

Yanping Yang[1], Jaclyn E. McCloskey[1], Huan Yang[2], Janusz Puc[2], Yago Alcaina[1], Yogindra Vedvyas[1], Angel A. Gomez Gallegos[1,3], Elizabeth Ortiz-Sánchez[3], Elisa de Stanchina[4], Irene M. Min[5], Eric von Hofe[2], and Moonsoo M. Jin[1,4]

ABSTRACT

Adoptive transfer of chimeric antigen receptor (CAR) T cells has demonstrated unparalleled responses in hematologic cancers, yet antigen escape and tumor relapse occur frequently. CAR T-cell therapy for patients with solid tumors faces even greater challenges due to the immunosuppressive tumor environment and antigen heterogeneity. Here, we developed a bispecific CAR to simultaneously target epithelial cell adhesion molecule (EpCAM) and intercellular adhesion molecule 1 (ICAM-1) to overcome antigen escape and to improve the durability of tumor responses. ICAM-1 is an adhesion molecule inducible by inflammatory cytokines and elevated in many types of tumors. Our study demonstrates superior efficacy of bispecific CAR T cells compared with CAR T cells targeting a single primary antigen. Bispecific CAR T achieved more durable antitumor responses in tumor models with either homogenous or heterogenous expression of EpCAM. We also showed that the activation of CAR T cells against EpCAM in tumors led to upregulation of ICAM-1, which rendered tumors more susceptible to ICAM-1 targeting by bispecific CAR T cells. Our strategy of additional targeting of ICAM-1 may have broad applications in augmenting the activity of CAR T cells against primary tumor antigens that are prone to antigen loss or downregulation.

Introduction

Chimeric antigen receptor (CAR) T-cell therapy is a rapidly emerging immunotherapy approach which reprograms T-cell specificity and function using a synthetic antigen receptor (1, 2). Adoptive transfer of CAR T cells has produced remarkable responses across a range of B-cell leukemias and lymphomas, in which all other treatment options have been exhausted (3–5). Early clinical trial results also indicate encouraging clinical efficacy of CAR T-cell therapy against relapsed or refractory multiple myeloma (6, 7). In spite of high rates of initial response with anti-CD19 CAR T cells, however, relapses involving diminished or complete loss of cell surface antigen, typically within 1 year of treatment, are observed in approximately 30% to 50% of patients who have remission (8–10). Relapses associated with antigen loss have also been reported with CARs directed against other targets such as CD22 and B-cell maturation antigen (BCMA), underscoring antigen escape as a significant and common impediment to the success of CAR T-cell therapy (6, 7, 11). Going beyond hematologic cancers, antigen escape is likely to be an even greater challenge for CAR T-cell therapy against solid tumors, which are generally composed of cells with heterogeneous antigen expression (12–14).

One particular strategy to circumvent antigen escape is to target multiple tumor antigens simultaneously and thereby reduce the risk of relapse. A phase I clinical trial with bispecific CD19–CD20 CAR T cells has demonstrated substantial efficacy against relapsed, refractory B-cell malignancies (15). Tandem CD19–CD22 and CD19–CD123 CAR T cells have also been shown to enhance T-cell functionality and reduce antigen escape in preclinical models (11, 16), and the CD19–CD22 CAR is currently being tested in humans (ClinicalTrials.gov Identifier: NCT03241940 and NCT03448393). Likewise, multispecific targeting has demonstrated potential to overcome the antigen heterogeneity in solid tumors. For instance, a tandem CAR that can simultaneously target HER2 and IL13Rα2 mitigated antigen escape and showed improved antitumor efficacy over T cells with a monospecific CAR, a pooled CAR T product, or T cells coexpressing two separate CARs (17). Therefore, multispecific targeting might provide an effective means to overcome antigen escape and potentially bring a significant advance to the field.

ICAM-1 is a transmembrane glycoprotein with cytokine-inducible nature and long known for its important role in facilitating leukocyte endothelial transmigration (18, 19). ICAM-1 is constitutively present at low levels on endothelial cells and leukocytes; however, its expression can be significantly upregulated upon stimulation by inflammatory mediators such as IL1, IFNγ, TNFα, and lipopolysaccharide (19). When upregulated, the interaction between ICAM-1 and lymphocyte function–associated antigen-1 (LFA-1) on leukocytes promotes the immobilization and extravasation of leukocytes from circulation. ICAM-1 overexpression has been observed across various types of tumors and the associated stroma (20–22) and has been implicated in tumor progression and drug resistance (23, 24). Clinical studies using mAbs suggest the suitability and tolerability of ICAM-1 targeting (25, 26). Previously, we developed a low-affinity CAR (F292A CAR, $K_d \approx 20$ μmol/L) specific to ICAM-1 through a process called "affinity-tuning," which renders CAR T cells to be selective to tumors

[1]Molecular Imaging Innovations Institute, Department of Radiology, Weill Cornell Medicine, New York, New York. [2]AffyImmune Therapeutics, Inc., Natick, Massachusetts. [3]Subdirección de Investigación Básica, Instituto Nacional de Cancerología, Ciudad de México, México. [4]Antitumor Assessment Core Facility, Memorial Sloan Kettering Cancer Center, New York, New York. [5]Department of Surgery, Weill Cornell Medicine, New York, New York.

Note: Supplementary data for this article are available at Cancer Immunology Research Online (http://cancerimmunolres.aacrjournals.org/).

Corresponding Author: Moonsoo M. Jin, Department of Radiology, Weill Cornell Medicine, New York, NY 10065. Phone: 646-962-6115; E-mail: moj2005@med.cornell.edu

Cancer Immunol Res 2021;XX:XX–XX

doi: 10.1158/2326-6066.CIR-21-0062

Published OnlineFirst August 2, 2021; DOI: 10.1158/2326-6066.CIR-21-0062

with overexpressed antigens, while sparing normal cells with basal expression (27, 28). These micromolar affinity ICAM-1 CAR T cells are currently being evaluated for safety and preliminary efficacy in patients with advanced thyroid cancer (NCT04420754).

In an effort to expand CAR T-cell therapy against other indications and tumor antigens, we have chosen a molecule called EpCAM as a tumor target antigen and built a CAR using a previously isolated synthetic antibody called UBS54 (29). EpCAM is a surface antigen that has been found to be frequently upregulated in a wide variety of carcinomas, including colorectal, gastric, pancreatic, and endometrial cancers (30). With the intention of developing CAR T cells that are more resistant to antigen escape, we sought to generate a bispecific CAR that can target EpCAM and ICAM-1 simultaneously. We hypothesized that complementing EpCAM CAR with additional targeting of ICAM-1, owing to the inducible nature of ICAM-1 by inflammatory T-cell cytokines, will improve the efficacy of CAR T cells against the EpCAM-overexpressing tumors and prevent the immune evasion of antigen-negative variants. Our data demonstrate that EpCAM-specific CAR T cells alone were able to robustly eradicate multiple solid tumors but were susceptible to relapse. In contrast, bispecific dual CAR T cells that additionally targeted ICAM-1 showed a potential of preventing tumors from becoming resistant or reducing relapse of tumors with heterogeneous EpCAM expression. The addition of ICAM-1 targeting significantly elevated the antitumor activity of CAR T cells, even when tumors had little ICAM-1 expression prior to treatment. We showed that ICAM-1 can be induced by proinflammatory cytokines secreted upon CAR interaction with the primary antigen, that is, EpCAM, rendering tumor cells more vulnerable to the dual CAR T cells.

Materials and Methods

Cell culture

The human glioblastoma cell line U-251 (a kind gift from B. Law, Weill Cornell Medicine, New York, NY) and human thyroid cancer cell line 8505C were purchased from Sigma in 2018. Gastric cancer cell line MKN-45 was purchased from DSMZ in 2016, whereas SNU-638 was obtained in 2018 from the Korean Cell Line Bank (Seoul National University, Seoul, Republic of South Korea). The human breast cancer cell lines MDA-MB-231 and SK-BR-3 (a kind gift from J. Babich, Weill Cornell Medicine, New York, NY), pancreatic cancer cell lines SW-1990 and Capan-2, colon cancer cell line HT-29, gastric cancer cell line Hs 746T, 293T and Jurkat cell lines were purchased from the ATCC from 2018 to 2020. U251, MDA-MB-231, SW-1990, Hs 746T, and 293T were cultured in DMEM (Corning) supplemented with 10% FBS; SK-BR-3, Capan-2, and HT-29 were maintained in McCoy's 5A (ATCC) containing 10% FBS; 8585C, MKN-45, and SNU-638 were maintained in RPMI1640 (Corning) supplemented with 10% FBS. All tumor cells were transduced with a Firefly Luciferase-F2A-GFP (FLuc-GFP) lentivirus (Biosettia) for bioluminescence-based cytotoxicity and mouse imaging experiments. Human primary colonic (H-6047), kidney (H-6034), and liver (H-6044) epithelial cells isolated by magnetic activated cell sorting using EpCAM-specific antibodies were obtained from Cell Biologics, Inc. in 2019 and were maintained in complete human epithelial cell medium (Cell Biologics, Inc., catalog no. H6621) according to the vendor's recommendations. All cells were cultured in a humidified incubator at 37°C with 5% CO_2 and were routinely tested for mycoplasma using a MycoAlert detection kit (Lonza). Cell lines were used for *in vitro* and *in vivo* experiments with a maximum of 20 passages, whereas primary epithelial cells were used for assays within three passages.

CRISPR–Cas9 editing of cell lines

EpCAM-knockout cell lines were generated using the Alt-R CRISPR-Cas9 System (Integrated DNA Technologies, Inc.) according to the manufacturer's instructions. Trans-activating CRISPR RNA (tracrRNA) and CRISPR RNA (crRNA) oligos were annealed in equimolar concentrations by heating at 95°C for 5 minutes, followed by gradual cooling to room temperature. Two crRNAs were used to target two exons of EpCAM: crRNA-AA, 5′-rGrArU rCrArC rArArC rGrCrG rUrUrA rUrCrA rArCrG rUrUrU rUrArG rArGrC rUrArU rGrCrU-3′; crRNA-AB, 5′-rGrUrG rCrArC rCrArA rCrUrG rArArG rUrArC rArCrG rUrUrU rUrArG rArGrC rUrArU rGrCrU-3′. Guide RNA duplex (22 pmol) was then incubated with Cas9 nuclease (18 pmol) at room temperature for 20 minutes to form the ribonucleoprotein (RNP) complex. A total of 5×10^4 cells were mixed with RNP-AA and RNP-AB complexes into a 10 μL Neon tip. The final concentration for each electroporation was 1.8 μmol/L gRNA-AA, 1.8 μmol/L gRNA-AB, and 1.5 μmol/L Cas9 nuclease. After electroporation (1,250 V/20 ms/3 pulses) using the Neon Transfection System (Invitrogen), cells were immediately transferred to a 24-well plate containing 0.5 mL of prewarmed culture medium (RPMI, 10% FBS), and incubated in a humidified 37°C, 5% CO_2 incubator. Five days later, EpCAM expression on cell surface was assessed by flow cytometry (details in the "Flow cytometry" section).

Lentiviral vector construction

EpCAM-specific CAR constructs and the negative control BCMA CAR construct were synthesized and cloned by GenScript into a lentiviral plasmid backbone (VectorBuilder Inc., Vector Design Studio) under the regulation of a human elongation factor 1α (EF1α) promoter. EpCAM-specific single CAR contains single-chain variable fragment (scFv) derived from anti-EpCAM mAb UBS54 (29), whereas BCMA-specific CAR contains the scFv derived from J22.9-xi antibody (31). Coding sequences of scFv were inserted into the second-generation CAR construct containing from the 5′-LTR end: EF1α promoter, signal sequence, c-Myc tag, scFv, CD8 hinge, transmembrane and cytoplasmic domains of CD28, and the cytoplasmic domain of CD3ζ. The PET reporter gene SSTR2 was incorporated after CAR following a "self-cleaving" ribosome-skipping porcine teschovirus-1 2 A (P2A) sequence. For the bicistronic dual CAR, UBS54 scFv was appended to CD28–CD3ζ while F292A I domain to 4-1BB–CD3ζ. A c-Myc or Flag tag was introduced at the N-terminus of each CAR for the detection of CAR expression. Both CARs were coexpressed in a tricistronic construct with SSTR2 via P2A and thosea asigna virus 2A (T2A) ribosome-skipping sequences.

CAR T-cell manufacturing

Lentivirus was packaged by VectorBuilder and frozen at −80°C until use. Jurkat T cells were transduced by an overnight incubation with the lentivirus at 1:25 dilution, and the expression of the CAR was validated after 3 days by flow cytometry. Human leukopaks from four heathy donors were commercially obtained from Biological Specialty Corporation between 2018 and 2019. T cells were enriched to obtain >95% CD3 purity by magnetic activated cell sorting using human CD4 (Miltenyi Biotec, catalog no. 130-045-101) and human CD8 (Miltenyi Biotec, catalog no. 130-045-201) MicroBeads. CD4/CD8-enriched T cells were activated with human T-activator CD3/CD28 Dynabeads (Gibco) at a bead-to-cell ratio of 1:1 and cultured in complete T-cell growth medium: TexMACS medium (Miltenyi Biotec) containing 5% human AB serum (Sigma), IL7 (12.5 ng/mL; Miltenyi Biotec), and IL15 (12.5 ng/mL; Miltenyi Biotec). T-cell transduction with lentivirus (1:25 dilution) was performed twice at 24 and 48 hours after activation.

Published OnlineFirst August 2, 2021; DOI: 10.1158/2326-6066.CIR-21-0062

T cells were expanded in 50 mL bioreactor tubes (TubeSpin, TPP) at $1-3 \times 10^6$ cells/mL on a tube roller (Thermo Fisher Scientific) with a setting of 5 rpm. Transduction efficiency was evaluated by flow cytometry on days 6 to 7 after T-cell activation. On day 10, cell products were cryopreserved in a 1:2 mixture of T-cell complete growth medium and CS10 (STEMCELL) for *in vitro* and *in vivo* experiments.

Determination of CAR affinities

Recombinant human monomeric EpCAM (R&D Systems, catalog no. 9277-EP-050), human EpCAM-Fc (R&D Systems, catalog no. 960-EP-050), and mouse EpCAM-Fc (R&D Systems, catalog no. 9364-EP-100) were conjugated with either Alexa Fluor 488 or Alexa Fluor 647 using a labeling kit (Thermo Fisher Scientific, catalog nos. A30006 and A30009) to determine the relative binding of soluble EpCAM to CAR molecules expressed on Jurkat T cells. In the saturation binding assay, 5×10^4 UBS54 CAR T cells or nontransduced T (NT) cells were added in triplicate to a 96-well plate and washed with PBS containing 1% BSA. Cells were then stained at 4°C for 15 minutes with 2-fold serially diluted Alexa Fluor 647–conjugated monomeric EpCAM protein starting from 2 μmol/L. Flow cytometry was performed on a Gallios flow cytometer (Beckman Coulter, Inc.) and analyzed using the FlowJo software (Tree Star, Inc.). The mean fluorescence intensities (MFI) were used to calculate the equilibrium dissociation constant (K_d) using the one-site nonlinear regression model (GraphPad Prism 8).

Cytotoxicity assays

Bioluminescence-based cytotoxicity assays were performed against firefly luciferase–expressing tumor target cells including U-251, MDA-MB-231, SW-1990, MKN-45, SK-BR-3, Capan-2, HT-29, SNU-638, 8505C, 293T, and Hs 746T. A total of 5×10^3 target cells were co-cultured with NT, UBS54, F292A, or dual CAR T cells in 96-well plates at indicated effector-to-target (E:T) ratios. Cocultures were performed in T-cell growth media containing D-luciferin (150 μg/mL; Gold Biotechnology) without any cytokine supplement. Luminescence was measured by a microplate reader (TECAN Infinite M1000PRO) at indicated time points. The percentage of viability was calculated by dividing relative luminescence units (RLU) by that of target cells only. The percent lysis was calculated by the following equation: percentage = [(target cells only RLU − test RLU)/target cells only RLU] × 100. For real-time cytotoxicity assays against primary colon, kidney, and liver epithelial cells, an xCELLigence Real Time Cell Analyzer (Agilent) was used to record the cell index at 15-minute intervals. A total of 5×10^3 NT or UBS54 CAR T cells were added to a 96-well E-plate preseeded with 5×10^3 target cells overnight. Cocultures were performed in T-cell growth media without any cytokine supplement. The percentage of lysis was generated by RTCA software using the formula: %Lysis = [(target cells only cell index − test cell index)/target cells only cell index] × 100. Data were presented as the mean ± SD of triplicate wells.

In vivo mouse studies

Four to 6 weeks old male NOD.Cg-Prkdc^{scid} Il2rg^{tm1Wjl}/SzJ (NSG) mice were purchased from the Jackson Laboratory, and housed in the Animal Core Facility at Weill Cornell Medicine (New York, NY). All animal studies were reviewed and approved by Weill Cornell Medicine Institutional Animal Care and Use Committees. Peritoneal gastric cancer models were established by injecting 0.5×10^6 FLuc-expressing SNU-638 tumor cells into the peritoneal cavity. After 7 days, control NT cells or anti-EpCAM UBS54 CAR T cells (10×10^6 cells/mouse) were injected intraperitoneally. For systemic gastric cancer models, both MKN-45-FLuc$^+$ tumor cells (0.5×10^6 cells/mouse), NT and UBS54 CAR T cells (10×10^6 cells/mouse) were injected via tail vein. T cells were administered 5 days after tumor inoculation. The orthotopic pancreatic tumor models were established by surgical implantation of Capan2-FLuc$^+$ cells at a density of 0.1×10^6 cells in 25 μL of 1:1 mixture of McCoy's 5A and Matrigel (Corning). Fifteen days later, NT and UBS54 CAR T cells were injected intravenously via tail vein (10×10^6 cells/mouse). Patient-derived xenograft (PDX) models were generated by Antitumor Assessment Core Facility at Memorial Sloan Kettering Cancer Center as described previously (32). Seven days after inoculation of passage 3 tumors, mice were treated with 10×10^6 NT or CAR T cells via tail vein.

For subcutaneous tumor models using cell lines, wild-type SNU-638 or a heterogenous population of SNU-638 (90% wild-type, 10% EpCAM-knockout) or MKN-45 (90% wild-type, 10% EpCAM-knockout) tumor cells (1×10^6 cells/mouse) were implanted subcutaneously into the upper left flank of NSG mice. Five or 7 days later, mice were treated with 10×10^6 NT, UBS54 CAR T, or dual CAR T cells via intravenous injection. Mouse blood was collected from retro-orbital plexus after treatment at indicated time points. Plasma supernatants were harvested following centrifugation at 1,000 × *g*, 4°C for 15 minutes and stored at −80°C for cytokine analysis. Tumors were collected at the indicated time points to measure EpCAM and ICAM-1 expression by flow cytometry or IHC as described below.

To evaluate toxicity *in vivo*, we established a bilateral tumor model by subcutaneously implanting 1×10^6 SW-1990 cells on the left flank and 1×10^6 SNU-638 cells on the right flank. The SW-1990 cell line was selected to model physiologic levels of EpCAM expression on normal tissues, and SNU-638 was chosen as a representative EpCAM-overexpressing tumor. Seven days after tumor inoculation, mice were treated with UBS54 CAR or negative control BCMA CAR T cells (10×10^6 cells/mouse) via tail vein injection.

All T cells were cryopreserved and used for injection freshly after thawing. Tumor growth was monitored weekly using an IVIS Spectrum *in vivo* imaging system (PerkinElmer). Bioluminescence images were acquired 15 minutes after intraperitoneal injection of 200 μL of 15 mg/mL D-luciferin (Gold Biotechnology). For the peritoneal SNU-638 tumor model, D-luciferin was injected subcutaneously. Whole-body bioluminescence flux was used to estimate tumor burden. For subcutaneous tumors, tumor volume (V) was measured with a caliper on a weekly basis and calculated using the formula $V = [\text{length} \times (\text{width})^2]/2$. PET/CT imaging was performed to track T-cell biodistribution using a micro-PET/CT scanner (Inveon, Siemens) 2 hours after intravenous injection of ^{18}F-NOTA-OCT tracer (1,4,7-Triazaclononane-1,4,7-triacetic acid-octreotide). Randomization of mice was performed on the basis of bioluminescent imaging or tumor size measurements to ensure tumor establishment prior to treatment. The health condition of mice was monitored on a daily basis by the veterinary staffs, independent of the investigators and studies. Euthanasia was applied when a humane endpoint had been reached (e.g., >25% body weight loss, signs of illness or distress including ruffled fur, difficulty with diet, or abnormal posture). Investigators were not blinded when monitoring mice survival. If a mouse died during imaging processes, with no prior sign of tumor progression, then it was considered a tumor-unrelated death, and the mouse was indicated as censored in survival analysis.

Cell isolation from tumors

Tumor tissues were cut into small pieces of 2 to 4 mm and digested at 37°C for 1 hour in 5 mL of RPMI1640 medium supplemented with 10% FBS, collagenase type IV (200 U/mL, Gibco), and DNase I

Published OnlineFirst August 2, 2021; DOI: 10.1158/2326-6066.CIR-21-0062

(100 U/mL, New England BioLabs, Inc.). Samples were then triturated using a serological pipet and strained through a 70 μm cell strainer to generate single-cell suspensions. Red blood cells were lysed in ACK lysis buffer (Lonza) for 5 minutes, and excess debris was removed using a debris removal solution (Miltenyi Biotec). EpCAM and ICAM-1 expression in tumor cells was assessed by flow cytometry as described below.

Flow cytometry

Flow cytometry data were acquired on a Gallios flow cytometer (Beckman Coulter, Inc.) and analyzed using the FlowJo software (Tree Star, Inc.). Prior to staining, cells were washed with PBS containing 1% BSA and blocked with mouse IgG (200 μg/mL; Sigma-Aldrich). Cell staining was conducted at room temperature or at 4°C for 15 minutes. Cells were washed twice and then resuspended in 200 μL PBS containing 1% BSA for analysis on flow cytometer. Tumor cell surface markers were determined with the following antibodies: PE-Cy7 anti-human CD326 (EpCAM; BioLegend, clone 9C4) and APC anti-human CD54 (ICAM-1; BioLegend, clone HA58). For CAR detection and T-cell phenotypic analysis, the following antibodies were used: FITC anti–c-myc (Miltenyi Biotec, clone SH1-26E7.1.3), APC anti-human SSTR2 (R&D Systems, clone 402038), anti-human PE-Cy5 CD3/PE CD4/FITC CD8 cocktail (BioLegend, clone UCHT1; RPA-T4; RPA-T8), PE-Cy7 anti-human CD137 (4-1BB; BioLegend, clone 4B4-1), APC anti-human CD69 (BioLegend, clone FN50), PE-Cy7 anti-human CD152 (CTLA-4; BioLegend, clone BNI3), PE-Cy7 anti-human CD223 (LAG-3; BioLegend, clone 11C3C65), APC anti-human CD336 (TIM-3; BioLegend, clone F38-2E2), and Brilliant Violet 421 anti-human CD279 (PD-1; BioLegend, clone EH12.2H7). Calcein Blue (Sigma-Aldrich, catalog no. M1255) staining along with forward- and side-scatter gating was used to exclude dead cells. For the staining of tumor cells or T cells isolated from *in vitro* cocultures, 1×10^5 NT, F292A, UBS54, or dual CAR T cells were coincubated for 24 hours with 1×10^5 target cells [U-251, MDA-MB-231, SW-1990, MKN-45 (wild-type or heterogenous mixture), SK-BR-3, Capan-2, HT-29, SNU-638 (wild-type or heterogenous mixture), 8505C, 293T, and Hs 746T]. Cells were then isolated, washed, and stained with EpCAM, ICAM-1, CD3, CD137, and CD69 antibodies. GFP^+ cells were gated as tumor cells, whereas $CD3^+$ cells were gated as T cells. The general flow cytometry gating strategies are shown in Supplementary Fig. S1.

IHC

IHC staining was performed with the following antibodies: anti-human EpCAM (Cell Signaling Technology, clone D1B3), anti-EGFP (LSBio, catalog no. LS-C757212), and anti-human CD3 (LSBio, clone CD3-12). For tumor samples from mouse models, tissues were fixed in 10% neutral buffered formalin (Azer Scientific) overnight and stored in 70% ethanol until submitting to IHC World for embedding, sectioning, and staining. Paraffin-embedded PDX sections derived from 3 patients with gastric cancer were kindly provided by Antitumor Assessment Core Facility and processed for histology by Molecular Cytology Core Facility at Memorial Sloan Kettering Cancer Center (New York, NY). Stained slides were scanned by HistoWiz and analyzed using Aperio ImageScope (Leica Biosystems).

Cytokine analysis

A total of 5×10^3 NT, UBS54, F292A or dual CAR T cells in T-cell growth medium without cytokine were cocultured with target cells (U-251, MDA-MB-231, SW-1990, MKN-45, SK-BR-3, Capan-2, HT-29, or SNU-638) in 96-well plates at an E:T ratio of 1:1. After 24 hours of incubation at 37°C, culture supernatants were collected and diluted 1:10 with culture medium. Cytokine secretion was measured by a Bio-Plex Pro human cytokine panel (Bio-Rad) or a custom LEGENDplex panel (BioLegend) according to the manufacturers' instructions. Mouse sera from gastric cancer PDX models, subcutaneous SNU-638, and MKN-45 (90% $EpCAM^+$) models were harvested at indicated time points after CAR T-cell treatment and analyzed by a custom LEGENDplex panel (BioLegend). Sera were diluted 1:2 with assay buffer before analysis. Sera from untreated mice were used as controls. Cytokine concentrations were calculated using a standard curve (standards provided within the kits) following the manufacturers' instructions.

Statistical analysis

Unpaired, two-tailed Student *t* test was performed to compare two groups. For multiple comparison analysis, ANOVA (one- or two-way) was used to evaluate statistical significance. When multiple groups were compared over multiple time points, statistical significance was determined by two-way ANOVA with Tukey multiple comparisons test. Mouse survival curves were generated using the method of Kaplan–Meier, and the significance was analyzed with the log-rank (Mantel–Cox) test. All statistical analyses were performed using Prism 8 (GraphPad, Inc.). $P < 0.05$ was considered statistically significant.

Results

CAR expression and affinity determination of the EpCAM CAR

We developed an anti-EpCAM CAR construct based on the second-generation CAR backbone (CD28–CD3ζ), with the incorporation of scFv derived from UBS54, an anti-EpCAM mAb selected from a phage display library (**Fig. 1A**; ref. 29). To test the affinity of UBS54 CAR molecule, Jurkat T cells were transduced with a lentiviral vector and stained with serially diluted monomeric EpCAM. The K_d value of UBS54 CAR was found to be approaching micromolar affinity (~0.91 μmol/L; **Fig. 1B**), substantially lower than that of the corresponding parent antibody (K_d = 5 nmol/L; ref. 29). $CD4^+/CD8^+$ sorted primary T cells were transduced with lentivirus after stimulation with anti-CD3/CD28 dynabeads for 24 hours. In the CAR T-cell products, CAR expression was measured by flow cytometry using a c-Myc tag antibody (**Fig. 1C**). Both CAR T and NT cells after 10-day expansion were comprised mainly of effector memory cells (T_{EM}) and effector cells (T_E) with comparable CD4:CD8 ratios. The expression of several T-cell activation and exhaustion markers (CD137, CTLA-4, LAG-3, TIM-3, and PD-1) were also similar between CAR T and NT cells (**Fig. 1C**).

EpCAM CAR T cells exert potent cytolytic activity against EpCAM-overexpressing targets

We tested EpCAM expression in a panel of tumor cell lines by flow cytometry (**Fig. 1D**). SK-BR-3 (breast cancer), Capan-2 (pancreatic cancer), HT-29 (colon cancer), and SNU-638 (gastric cancer) cells overexpressed EpCAM, whereas MKN-45 (gastric cancer) and SW-1990 (pancreatic cancer) cells showed moderate EpCAM expression, MDA-MB-231 (breast cancer) expressed low EpCAM, and U-251 (glioblastoma) exhibited undetectable EpCAM expression. Cytolytic activity of the CAR T cells was assessed by coincubation with a panel of tumor target cells. UBS54 CAR T cells showed significantly greater cytotoxicity against target cells expressing high EpCAM (HT-29 and SNU-638), but mediated less killing of low-density EpCAM-expressing MDA-MB-231 cells (**Fig. 1E**; Supplementary Fig. S2). Target cell lysis was generally EpCAM dependent,

Published OnlineFirst August 2, 2021; DOI: 10.1158/2326-6066.CIR-21-0062

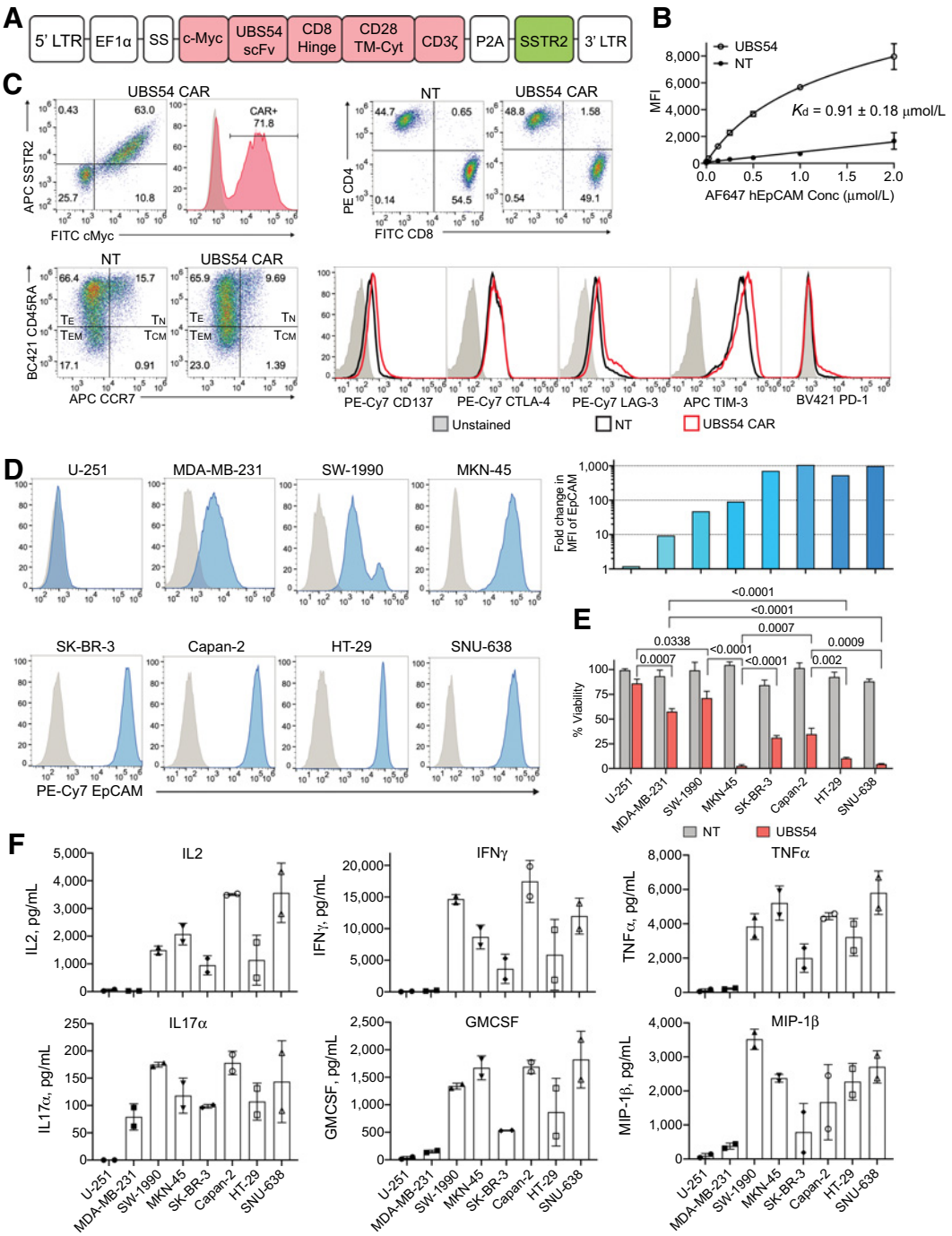

Figure 1.

The *in vitro* activity of EpCAM CAR T cells against tumor cell lines. **A,** Schematic representation of the lentiviral vector encoding EpCAM-specific UBS54 CAR. The expression of the CAR construct is driven by the EF1α promoter, and SSTR2 is placed following a ribosome-skipping sequence P2A. A c-Myc tag was introduced at the N-terminus for CAR detection. CD28 TM-Cyt, CD28 transmembrane and cytosolic domains; scFv, scFv derived from UBS54 mAb; SS, signal sequence. **B,** The affinity of the UBS54 CAR was determined by staining CAR-expressing Jurkat T cells with serially diluted EpCAM. K_d values were calculated using the one-site nonlinear regression model. Data represent mean ± SD (n = 3). **C,** Representative flow plots showing CAR expression, T-cell phenotypes (CD4, CD8, T_N CCR7$^+$CD45RA$^+$, T_{CM} CCR7$^+$CD45RA$^-$, T_{EM} CCR7$^-$CD45RA$^-$, T_E CCR7$^-$CD45RA$^+$), and activation and exhaustion markers (CD137, CTLA-4, LAG-3, TIM-3, and PD-1) in CAR T cells and NT. T_{CM}, central memory T cell; T_N, naïve T cell. **D,** Surface expression of EpCAM in tumor cell lines was determined by flow cytometry. EpCAM densities in tumor cell lines were presented as fold increases in EpCAM MFI normalized to unstained cells. **E,** Cytolytic activity of CAR T cells against EpCAM-expressing target cells and EpCAM-negative control U-251 cells. CAR T cells were coincubated with target cells at an E:T ratio of 1:1, and 24 hours later, the cell viability of target cells after CAR T-cell or NT treatment was normalized to that of the no T-cell control. Data represent mean ± SD (n = 3). Statistical significance was determined by unpaired, two-tailed t test. **F,** Cytokines in culture supernatants were measured after coincubation of CAR T cells and target cells for 24 hours (n = 2).

Published OnlineFirst August 2, 2021; DOI: 10.1158/2326-6066.CIR-21-0062

evidenced by the lack of killing of EpCAM-negative U-251 cells. However, cytotoxic activity of UBS54 CAR T cells was not fully dependent on EpCAM density in target cells, indicated by lower killing of EpCAM-high SK-BR-3 and Capan-2 cells, and close to complete killing of MKN-45 cells(intermediate EpCAM expression). The secretion of pro-inflammatory cytokines and chemokines (IL2, IFNγ, TNFα, IL17α, GMCSF, and MIP-1β) was absent against EpCAM-negative or EpCAM-low cells (U-251 and MDA-MB-231), and overall, specific to cytotoxic activity of UBS54 CAR T cells; however, the amount of cytokine release displayed variability above a threshold level of antigen density (**Fig. 1F**). Consistent with little activity against all cell lines, cytokine production by NT cells was below the lower limit of quantification (<0.5–10 pg/mL).

EpCAM-specific CAR T cells eliminate solid tumors in mouse models

After validation of CAR T-cell specificity against cell lines *in vitro*, we then examined UBS54 CAR T-cell activity in a peritoneal gastric cancer model using FLuc$^+$ SNU-638 tumor cells, an intestinal type of gastric cancer that shows microsatellite instability (33). This cell line has been used for screening anticancer drugs and in our previous study with ICAM-1–targeting CAR T cells (34, 35). NSG mice were inoculated intraperitoneally with SNU-638 cells and then treated 7 days later with NT or CAR T cells intraperitoneally (**Fig. 2A**). Untreated mice (No T) showed continued tumor growth in the intestinal tract and peritoneal cavity and expired within 60 days after tumor injection (**Fig. 2B–D**). NT cells slowed but did not control tumor growth, resulting in only marginal survival benefit. However, UBS54 CAR T cells rapidly eliminated tumors within 1 week after a single dose and prevented tumor relapse through the end of the study (125 days after tumor; **Fig. 2B–D**). All CAR T cell–treated mice remained healthy and survived without any signs of treatment-related toxicities (**Fig. 2D** and **E**).

Next, we evaluated UBS54 CAR T cells in a systemic gastric cancer model with MKN-45 tumor cells (**Fig. 2F**). MKN-45 cells were derived from a poorly differentiated gastric adenocarcinoma of medullary type, having the characteristics of both ordinary gastric mucosa and intestinal metaplastic mucosa (36). An intravenous injection of 0.5×10^6 MKN-45 cells initially formed tumor lesions in the lung, which quickly metastasized to liver, head, and joints. Untreated mice succumbed to the aggressive tumor growth approximately 30 days following tumor inoculation. Mice treated with NT cells had neither a treatment effect nor survival benefit over the No T cohort (**Fig. 2G–I**). In contrast, an equivalent number of CAR T cells led to complete tumor regression within 1 week after treatment and maintained complete responses in the majority of mice (**Fig. 2G–I**). Mice in the No T and NT cohorts showed a loss of body weight, whereas UBS54 CAR T cell–treated mice remained healthy and maintained stable body weight (**Fig. 2J**).

Finally, the efficacy of UBS54 CAR T cells was evaluated against pancreatic tumors, which frequently overexpress EpCAM, by surgically implanting 0.1×10^6 Capan2-FLuc$^+$ cells into mouse pancreas (**Fig. 2K**). Similar to the responses seen in the gastric cancer models, infusion of UBS54 CAR T cells led to rapid and durable tumor elimination, whereas tumors continued to grow in NT and No T cohorts (**Fig. 2L** and **M**). Body weight loss was observed in CAR T cell–treated mice, commencing after complete tumor eradication (**Fig. 2N**), likely due to GvHD (i.e., activation of human TCR against mouse tissue MHC). The UBS54 CAR was confirmed to not bind murine EpCAM (**Fig. 2O**). Collectively, we demonstrated that UBS54 CAR T cells were effective in eliminating EpCAM$^+$ cancer cell lines implanted either intraperitoneally, systemically, or orthotopically into the pancreas.

EpCAM CAR T cells eradicate gastric tumors in PDX models

After observing durable and complete response of tumors to UBS54 CAR T cells in mice implanted with cancer cell lines, we next assessed CAR T-cell activity in PDX models, which more closely resemble clinical tumors. NSG mice were subcutaneously engrafted with gastric tumor specimens derived from 3 patients (PDX42, PDX44, and PDX55) who had moderate to high expression of membranous and cytoplasmic EpCAM expression (**Fig. 3A**). One week later, mice in each PDX model were randomized and assigned to three treatment cohorts: no treatment, 10×10^6 NT, or 10×10^6 UBS54 CAR T cells (**Fig. 3B**). PDX42 tumors grew aggressively and reached a volume of 3,000 mm^3 approximately 3 weeks after tumor inoculation (**Fig. 3C**). Infusion of NT cells slowed, but did not stop, tumor growth, and mice succumbed to tumors approximately 4 weeks after tumor inoculation. In contrast, a single dose of UBS54 CAR T cells suppressed the progression of aggressive PDX42 tumors and produced 100% tumor-free survival (**Fig. 3C** and **D**). PDX44 and PDX55 tumors grew relatively slower, reaching a volume of 1,000 mm^3 approximately 7 weeks following tumor implantation. In stark contrast to the progressive tumor growth in No T and NT cohorts, PDX44 and PDX55 were completely eradicated by 15 days after UBS54 CAR T-cell injection. The rapid response of tumors to CAR T-cell treatment was further corroborated by cytokine release following T-cell infusion. Serum IFNγ and perforin concentrations from UBS54 CAR T cell–treated mice peaked approximately 1 week after T-cell infusion and returned to background levels the following week when tumors were completely eradicated (**Fig. 3E**). Approximately 10 weeks after treatment, 2 of 4 tumor-free UBS54 CAR T cell–treated mice had a spike in serum cytokines due to GvHD-mediated T-cell expansion. We engineered CAR T cells to co-express human somatostatin receptor 2 (SSTR2; **Fig. 1A**), which functioned as a PET reporter for tracking CAR T-cell distribution spatially and temporally using a SSTR2-specific radiotracer [^{18}F-NOTA-Octreotide (37)]. PET/CT imaging revealed rapid accumulation of CAR T cells in the subcutaneous tumors, followed by subsequent contraction when tumors were eliminated on day 14 (**Fig. 3F**). In the NT-treated mice, subcutaneous tumors could be clearly detected by CT images and continued to grow with little tracer uptake. Taken together, these results further confirmed the potent antitumor activity of UBS54 CAR T cells against gastric tumors.

Dual targeting of EpCAM and inducible ICAM-1 promotes killing of heterogenous tumors

Heterogeneous antigen expression or antigen escape, especially in solid tumors, is increasingly recognized as a cause of tumor relapse and treatment failure. Here, we generated CRISPR–Cas9 EpCAM knockout tumor cell lines (Supplementary Fig. S3A) and mixed them with wild-type cell lines at defined ratios to mimic the degree of heterogeneity in EpCAM expression. After incubating a heterogeneous mixture of SNU-638 or MKN-45 cells (40%–60% EpCAM$^+$ each) with UBS54 CAR T cells for 24 hours, EpCAM$^+$ cells were eliminated from both populations, and EpCAM$^-$ tumor cells were largely spared (**Fig. 4A**). Whereas EpCAM expression remained unaltered either after incubation with NT cells or addition of IFNγ, ICAM-1 expression in SNU-638 and MKN-45 cells was significantly upregulated after addition of IFNγ (10 ng/mL) to the culture. Compared with IFNγ treatment, higher ICAM-1 induction was observed in the remaining

Published OnlineFirst August 2, 2021; DOI: 10.1158/2326-6066.CIR-21-0062

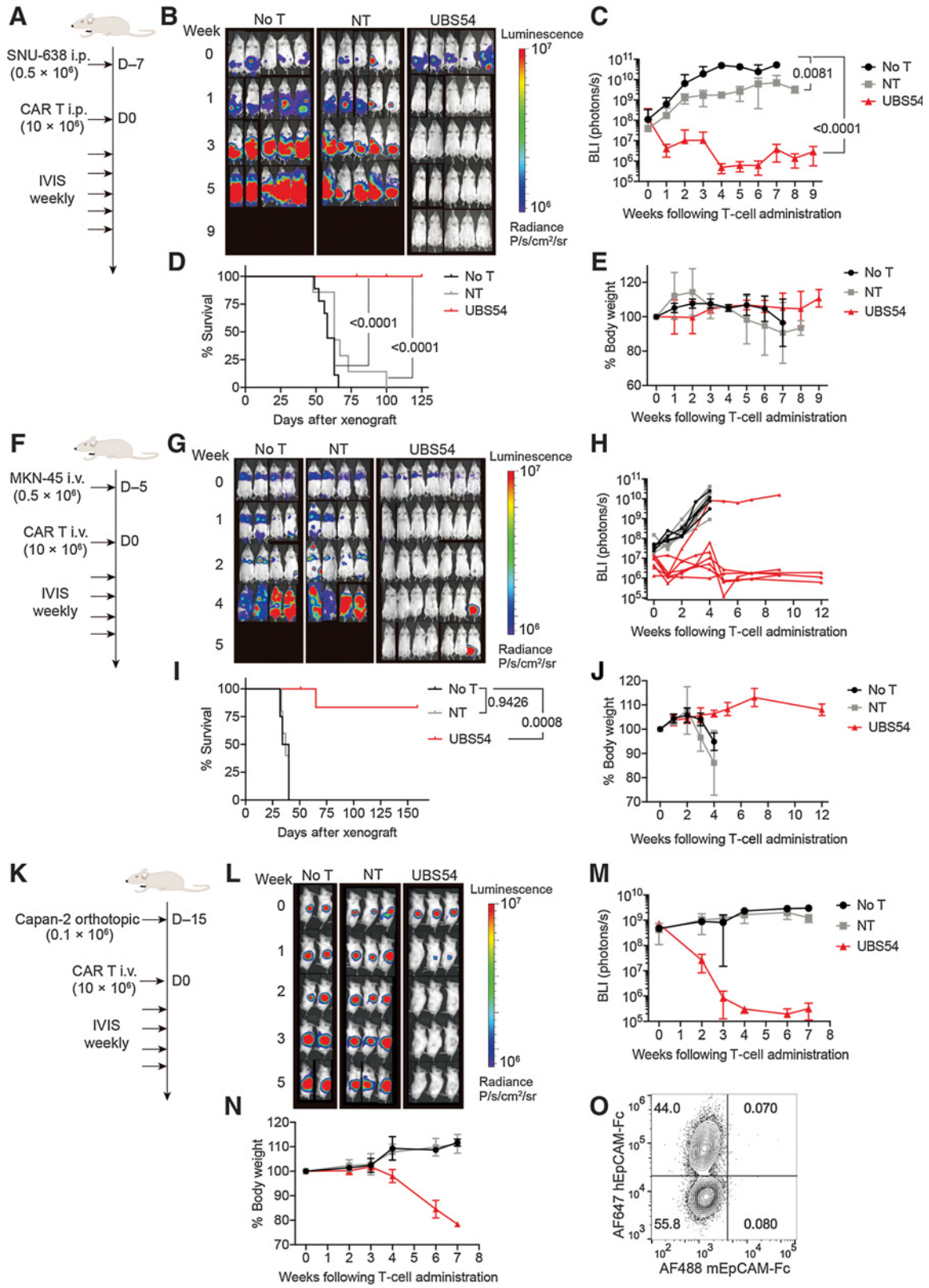

Published OnlineFirst August 2, 2021; DOI: 10.1158/2326-6066.CIR-21-0062

EpCAM$^-$ SNU-638 and MKN-45 cells after the EpCAM$^+$ cells were eliminated by CAR T cells (**Fig. 4A**; Supplementary Fig. S3B).

To broaden CAR T-cell efficacy against tumor cells with heterogenous EpCAM expression, we designed a bicistronic dual CAR that incorporates sequences of UBS54 scFv and affinity-tuned LFA-1 I domain [F292A, $K_d \approx 20$ μmol/L (27)] into one lentiviral vector (**Fig. 4B**). Costimulatory domains of CD28 and 41BB were used for EpCAM-specific and ICAM-1–specific CARs, respectively. The expression of UBS54 and F292A CAR in T cells was confirmed by flow cytometry using antibodies against c-Myc and Flag tags, which were fused at the N-terminus to UBS54 and F292A, respectively (**Fig. 4C**). We first measured the *in vitro* cytolytic activity of F292A, UBS54, and dual CAR T cells against SNU-638 or MKN-45 with a mixture of EpCAM$^+$ and EpCAM$^-$ cells (100%, 50%, or 3% EpCAM$^+$). Micromolar affinity F292A CAR T cells induced 40% specific lysis of SNU-638 cells at 48 hours through interaction with ICAM-1, whereas it mediated almost no killing of MKN-45 cells that had low ICAM-1 expression (**Fig. 4D**; Supplementary Fig. S3C). UBS54 CAR T cells lysed approximately 90% of SNU-638 and MKN-45 wild-type cells that were 100% EpCAM$^+$. The amount of cell death caused by UBS54 CAR T cells against heterogenous populations was significantly higher than the percentage of EpCAM$^+$ cells, for example, approximately 80% lysis of 50% EpCAM$^+$ cells and 40% to 50% lysis of 3% EpCAM$^+$ cells. Additional killing of EpCAM$^-$ cells was not from nonspecific activity of UBS54 CAR T cells but likely due to bystander killing mediated by soluble factors such as FasL, TRAIL, or localized release of perforin and granzyme B by activated T cells (38). As expected, dual CAR T cells attained increased killing of SNU-638 cells compared with single CAR T cells (F292A or UBS54) due to its ability to interact with both EpCAM and ICAM-1 antigens. Such enhanced killing, however, was also observed against MKN-45, which was ICAM-1 low, and was completely unreactive to ICAM-1–specific CAR T cells. This should come from ICAM-1 expression in MKN-45 cells induced above the activation threshold of the ICAM-1–specific CAR after exposure to proinflammatory cytokines (**Fig. 4A**). Higher T-cell activation of the dual CAR was further evidenced by the induction of surface CD137 expression and quantitative measurement of cytokine production, which were highest in dual CAR T cells (**Fig. 4E** and **F**).

In addition to using tumor cells comprising a heterogenous population of EpCAM$^+$ and EpCAM$^-$ cells, we further compared single and dual CAR T cells using a panel of tumor cell lines with varying levels of EpCAM and ICAM-1 expression with respect to the kinetics of target cell lysis, ICAM-1 induction in target cells that remained viable after incubation with CAR T cells, and induction of CD69 as a measure of T-cell activation (Supplementary Fig. S4). We found both UBS54 single and dual CAR T cells were specific to EpCAM expression in target cells, evidenced by a lack of killing and little ICAM-1 induction in EpCAM-negative or EpCAM-low tumor cell lines (U251, 8505C, and 293T). As expected, the low-affinity F292A CAR T cells killed only ICAM-1-high SNU-638 cells but spared other cell lines with lower ICAM-1 expression. Single UBS54 CAR T cells were equally as potent as dual CAR T against the majority of target cells with intermediate to high EpCAM expression. Additional expression of ICAM-1 in EpCAM$^+$ target cells did not elevate the activity of dual CAR T cells over single UBS54 CAR T cells *in vitro*, indicating the dominance of the UBS54 CAR over the lower affinity F292A CAR.

Dual CAR T cells are superior against tumors with homogeneous antigen expression

We then examined the activity of single versus dual CAR T cells against the hard-to-treat subcutaneous SNU-638 tumor model. Mice were subcutaneously implanted with 1×10^6 SNU-638 tumor cells, and 7 days later treated with 10×10^6 UBS54 or dual CAR T cells (**Fig. 5A**). UBS54 CAR T cells were able to eliminate tumors at early time points [14 complete remission (CR), bioluminescence intensity (BLI) $\leq 2 \times 10^8$ photons/second) of 20 at 3 weeks after CAR T infusion, 70%], but tumor relapse occurred frequently (8 CR at 4–6 weeks, 40%; 5 CR at 8 weeks, 25%; **Fig. 5B–E**). In contrast, dual CAR T cells led to complete clearance of the tumors in 100% of the cases (10 CR of 10 at 3 weeks). After 6 weeks after T-cell infusion, 2 mice had tumor relapses, but the relapsed tumors remained small and stable, in contrast to the relapsed and rapidly progressing tumors in UBS54 CAR T cell–treated mice (**Fig. 5B–E**). To examine whether antigen downregulation occurred in the relapsed tumors, we analyzed EpCAM expression in tumor cells by flow cytometry. The relapsed tumors from UBS54 CAR T cell–treated mice had comparable EpCAM expression to tumors from untreated mice (**Fig. 5F**), confirming that altered antigen expression was not the cause for tumor resistance in this model. In contrast to comparable activity of single and dual CAR T cells against SNU-638 *in vitro* (Supplementary Fig. S3C and S4B), UBS54 single CAR T cells were more susceptible to relapse of EpCAM$^+$ solid tumors *in vivo*, whereas dual CAR T cells with additional targeting of ICAM-1 produced a significantly augmented antitumor response.

Serum cytokines were also measured weekly during the first 3 weeks following T-cell administration. Serum IFNγ and perforin peaked 1 week after T-cell infusion and dropped to background levels in the following weeks when tumors were eliminated (**Fig. 5G**). The dynamics of CAR T-cell distribution and expansion were also assessed by PET/CT imaging using ^{18}F-NOTA-OCT (**Fig. 5H**). UBS54 CAR T peaked 2 weeks after T-cell infusion and gradually contracted or

Figure 2.

EpCAM-specific CAR T cells mediate complete remission in gastric and pancreatic cancer models. **A,** Schematic of the intraperitoneal SNU-638 tumor model. NSG mice were intraperitoneally implanted with 0.5×10^6 SNU-638 cells. Seven days later, mice were either left untreated or treated with NT or UBS54 CAR T cells (10×10^6 cells/mouse) via intraperitoneal injection. **B,** Bioluminescence images of SNU-638–engrafted NSG mice ($n = 2$ independent experiments). **C,** Quantitation of total-body bioluminescence intensity (BLI) from the two independent experiments ($n = 7$–9). *P* values determined by two-way ANOVA with Tukey multiple comparisons test. **D,** Kaplan–Meier survival curves ($n = 7$–9). *P* values determined by log-rank (Mantel–Cox) test. **E,** Summary of body weight changes over time ($n = 7$–9). **F,** Schematic of the systemic MKN-45 tumor model. Five days after intravenous inoculation of 0.5×10^6 MKN-45 cells, mice were treated with CAR T cells or control cells (10×10^6 cells/mouse, i.v.) or left untreated. **G,** Whole-body bioluminescence images of MKN-45–engrafted NSG mice. **H,** Quantitation of total-body bioluminescence intensity. Data are displayed for each individual mouse from No T ($n = 4$), NT ($n = 5$), and UBS54 ($n = 7$) cohorts. **I,** Kaplan–Meier survival curves. *P* values determined by log-rank (Mantel–Cox) test. **J,** Summary of body weight changes over time ($n = 4$–7). **K,** Schematic of the orthotopic Capan-2 tumor model; 0.1×10^6 Capan-2 cells were implanted orthotopically into the pancreas, and after 15 days, mice received 10×10^6 NT or UBS54 CAR T cells intravenously. **L,** Whole-body bioluminescence images of Capan-2–engrafted NSG mice. **M,** Quantitation of total-body bioluminescence intensity ($n = 2$–3). **N,** Body weight changes over time ($n = 2$–3). **O,** Jurkat T cells expressing the UBS54 CAR were stained with 100 nmol/L human EpCAM-Fc and 100 nmol/L mouse EpCAM-Fc. For **C**, **E**, **J**, **M**, and **N**, data represent mean ± SD.

Published OnlineFirst August 2, 2021; DOI: 10.1158/2326-6066.CIR-21-0062

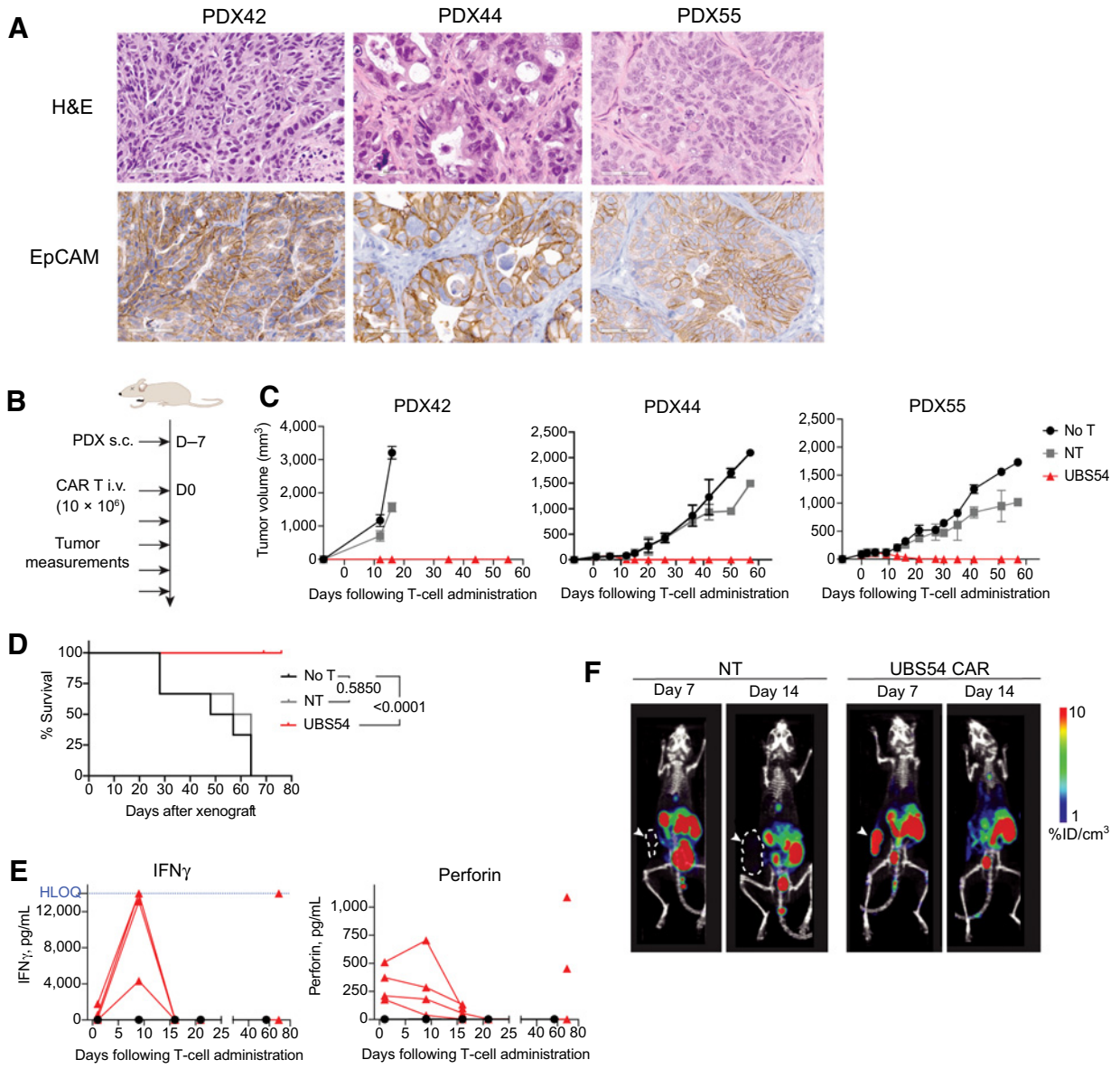

Figure 3.

UBS54 single CAR T cells control tumor growth in gastric cancer PDX models. **A,** EpCAM IHC staining and hematoxylin and eosin (H&E) staining on tumor sections from patients with gastric cancer (40× magnification; scale bar, 60 μm). **B,** Schematic of the gastric cancer PDX model. Allogeneic T cells from healthy donors were used. **C,** Tumor volumes in NSG mice without treatment (No T) or treated with NT or UBS54 CAR T cells ($n = 3$ for each PDX model). Data represent mean ± SD. **D,** Kaplan–Meier survival analysis of the three independent PDX experiments. Statistical significance was determined using log-rank (Mantel–Cox) test. **E,** Cytokines measured in mouse plasma at indicated time points after T-cell infusion. Data were pooled from independent PDX44 and PDX55 experiments and are shown as individual values ($n = 4$ mice). HLOQ, higher limit of quantification. **F,** PET/CT images showing CAR T-cell accumulation at tumor sites. Subcutaneous tumors are indicated by white arrowheads and dashed lines.

persisted over the next several weeks. In comparison, dual CAR T cells peaked earlier, and fully contracted by 3 weeks after T-cell infusion. The slower expansion and contraction kinetics of UBS54 CAR T cells were likely due to lingering interaction between CAR T cells and tumor cells. The systemic expansion of UBS54 CAR T cells outside of tumor implants was seen beginning 6 weeks after T-cell infusion (elevation of tracer uptake in lungs, thymus, and lymph nodes). In some mice with tumor relapse after treatment with UBS54 CAR T cells, CAR T-cell infiltration and expansion in tumors were apparent, indicating that tumor relapse was not attributable to poor infiltration and/or persistence but to potential T-cell dysfunction (**Fig. 5I**).

Additional ICAM-1 targeting complements EpCAM CAR T-cell activity against heterogenous tumors

We next examined whether additional targeting of ICAM-1 could complement EpCAM CAR T-cell activity against tumors with heterogenous EpCAM expression. To this end, we generated two gastric

Published OnlineFirst August 2, 2021; DOI: 10.1158/2326-6066.CIR-21-0062

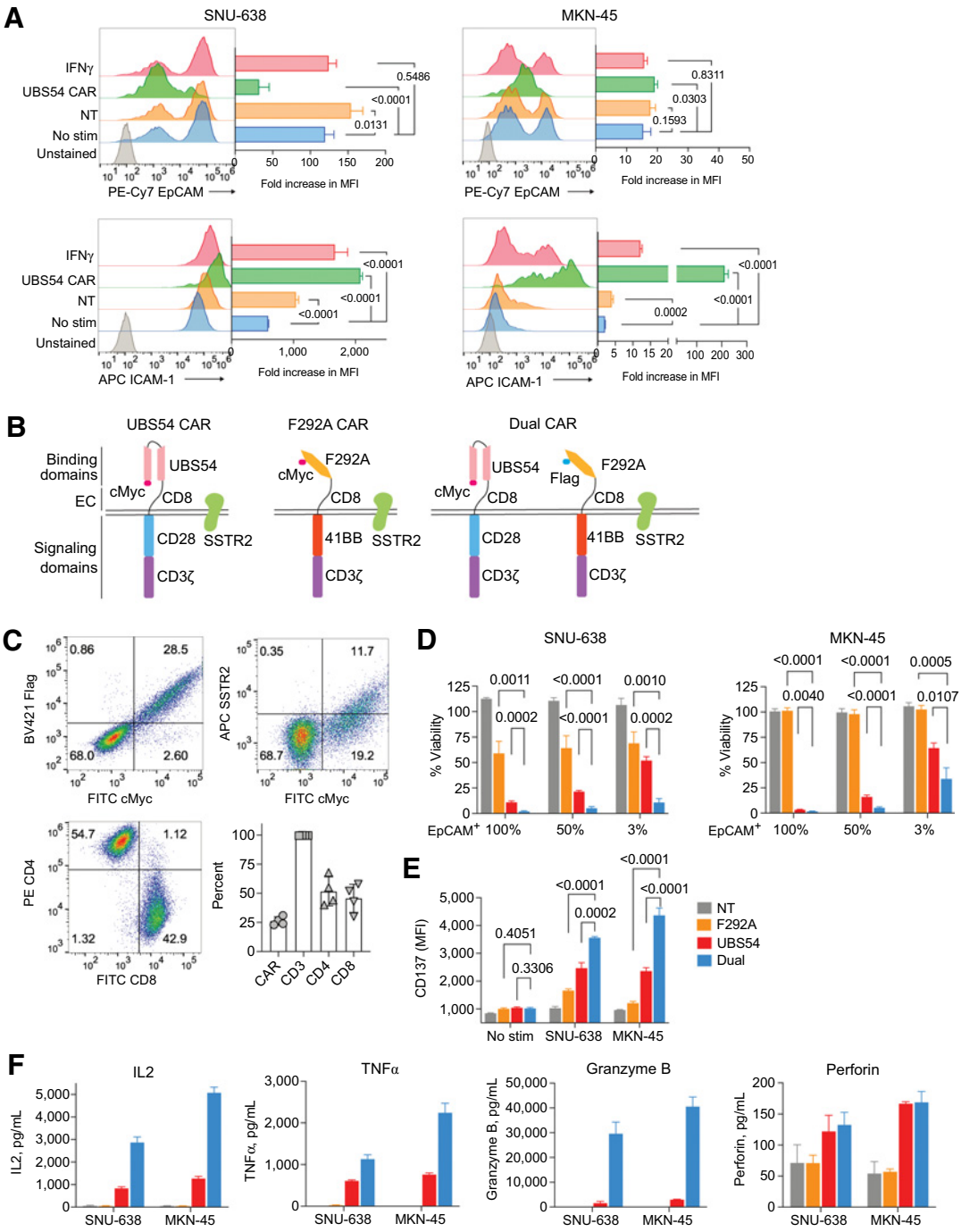

Figure 4.

Simultaneous targeting of EpCAM and ICAM-1 facilitates cytotoxicity against heterogenous tumor cell lines *in vitro*. **A,** A mixture of EpCAM$^+$ and EpCAM$^-$ SNU-638 or MKN-45 cells were treated with IFNγ (10 ng/mL) or coincubated with NT or UBS54 CAR T cells at an E:T ratio of 1:1. Surface EpCAM and ICAM-1 expression were evaluated by flow cytometry 24 hours later. Histogram represents fold increases in MFI normalized to unstained cells ($n = 4$). **B,** Schematic representation of the UBS54 and F292A unispecific CARs and bicistronic dual CARs. UBS54 scFv and LFA-1 I domain (F292A) were used for EpCAM and ICAM-1 targeting, respectively, with the fusion of a c-Myc or Flag tag for the detection of CAR molecules. EC, extracellular. **C,** Representative flow cytometry plots showing CAR expression and CD4/CD8 phenotype following transduction of human primary T cells. The production of dual CAR T cells was performed independently at least four times. The percentage of CAR-positive, CD3, and CD4/CD8 subsets is shown ($n = 4$). **D,** Bioluminescence-based cytotoxicity assay measuring cytolytic activity of F292A, UBS54, and dual CAR T cells. A heterogeneous population (100%, 50%, or 3% EpCAM$^+$) of SNU-638 or MKN-45 tumor cells were coincubated with T cells at an E:T ratio of 1:1 for 48 hours. The percentage of target cell viability was normalized to luminescence from the No T cohort ($n = 4$). Statistical significance was determined by unpaired, two-tailed *t* test. **E,** The upregulation of CD137 expression in T cells was measured after stimulation by SNU-638 or MKN-45 tumor cells (50% EpCAM$^+$) for 24 hours ($n = 4$). **F,** Cytokine production by NT, F292A, UBS54, and dual CAR T cells upon coculture with SNU-638 or MKN-45 tumor cells (50% EpCAM$^+$) for 24 hours ($n = 2$). For **A** and **C**–**F**, data represent mean ± SD.

Published OnlineFirst August 2, 2021; DOI: 10.1158/2326-6066.CIR-21-0062

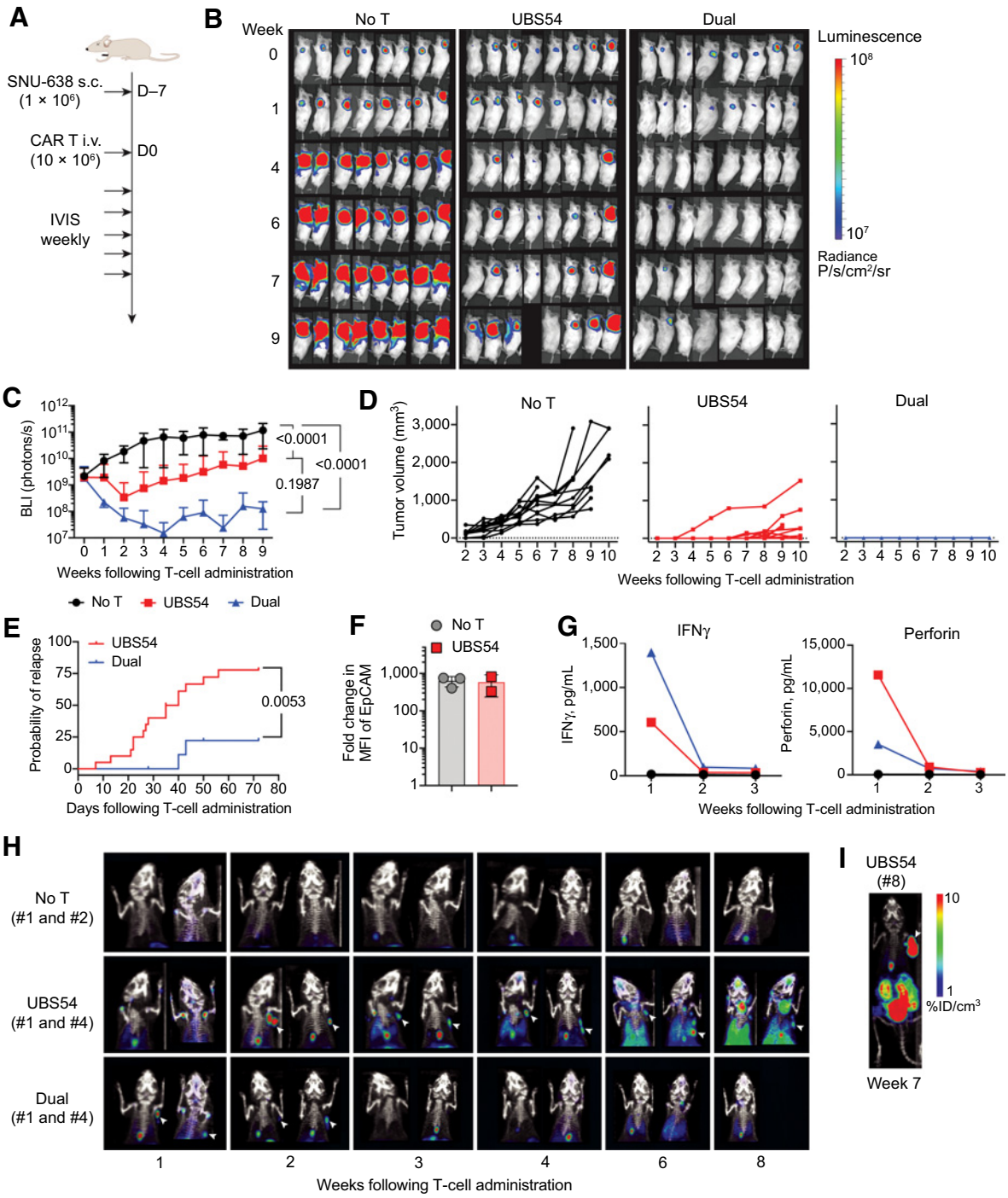

Figure 5.

EpCAM–ICAM-1 dual CAR T cells reduce tumor recurrence rate in a subcutaneous gastric cancer model. **A,** Schematic of the subcutaneous SNU-638 tumor model. NSG mice were subcutaneously implanted with 1×10^6 SNU-638 cells and treated 7 days later with UBS54 or dual CAR T cells (10×10^6 cells/mouse) via tail vein injection. **B,** Representative bioluminescence images of SNU-638–engrafted NSG mice. **C,** Quantitation of total-body bioluminescence intensity from independent experiments using three batches of donor-matched CAR T cells. Data are shown as mean ± SD (n = 10–20). Statistical significance determined by two-way ANOVA with Tukey multiple comparisons test. **D,** Tumor volumes for mice in the No T (n = 11), UBS54 (n = 20), and dual (n = 10) cohorts. **E,** Incidence of tumor relapse (total-body bioluminescence intensity > 2×10^8 photons/second, n = 10–20). P values determined by log-rank (Mantel–Cox) test. **F,** EpCAM cell-surface densities in relapsed tumors of mice sacrificed 8 to 12 weeks after UBS54 CAR T-cell treatment (mean ± SD, n = 2–3). Fold change in MFI of EpCAM was normalized to unstained cells. **G,** Serum IFNγ and perforin were measured weekly during the first 3 weeks following T-cell administration. **H,** Longitudinal PET/CT imaging to evaluate CAR T-cell expansion *in vivo* (n = 2/cohort). Subcutaneous tumors are indicated by white arrowheads. **I,** Representative PET/CT image showing CAR T-cell accumulation at tumors that relapsed or were resistant to UBS54 CAR T cells. The incidence of UBS54 CAR T-cell expansion in resistant tumors was observed in at least three independent experiments.

Published OnlineFirst August 2, 2021; DOI: 10.1158/2326-6066.CIR-21-0062

cancer tumor models by subcutaneously implanting a heterogeneous population of MKN-45 or SNU-638 tumor cells into NSG mice. In the MKN-45 model, which comprised tumors with 90% EpCAM$^+$ and 10% EpCAM$^-$ cells with little ICAM-1 expression (**Fig. 6A**), UBS-54 CAR T cells slowed tumor progression compared with the untreated cohort but failed to achieve tumor remission (**Fig. 6B–D**). As expected, F292A CAR T cells were ineffective against ICAM-1–low MKN-45 tumors. In comparison with F292A CAR T or UBS-54 CAR T cells, dual CAR T cells produced long-term regression and significant survival benefits (**Fig. 6B–E**). Three of 4 mice (75%) in the dual CAR T cohort attained CR 1 week following treatment. Of these, 1 mouse maintained a CR till the end of the study, whereas 2 mice developed tumor relapse. Relapsed MKN-45 tumors that were harvested from mice treated with UBS54 or dual CAR T cells revealed diminished EpCAM expression compared with untreated tumors, whereas resistant MKN-45 tumors harvested after F292A CAR T-cell treatment showed no difference in EpCAM expression (**Fig. 6F**). Consistent with the induction of ICAM-1 in CAR T cell–treated MKN-45 cells *in vitro* (**Fig. 4A**), MKN-45 tumors harvested from UBS54 or dual CAR T-cell cohorts showed more than 10-fold elevated expression of ICAM-1 (**Fig. 6F**). ICAM-1 upregulation rendered EpCAM$^+$ tumor cells more susceptible to killing by dual CAR T cells, resulting in tumor relapse or resistance of mainly EpCAM$^-$ICAM-1$^+$ tumors. We speculate that ICAM-1 expression induced in EpCAM$^-$ICAM-1$^+$ tumors was insufficient to drive full T-cell activation through the low-affinity F292A CAR in dual CAR T cells.

PET/CT imaging of CAR T cells revealed a pattern of CAR T-cell expansion and contraction in tumors (**Fig. 6G**), which has been noted to be a hallmark of efficient CAR T-cell elimination of tumors (37). However, in the UBS54 CAR T cell–treated mice, such biphasic kinetics of CAR T cells coincided with a persistent tumor mass revealed by CT imaging, caused by outgrowth of EpCAM$^-$ MKN-45 cells. In comparison, dual CAR T cells demonstrated an enhanced antitumor response against heterogenous tumors, which also resulted in a lower degree of CAR T-cell expansion. In the F292A CAR T-cell cohort, no specific tracer uptake was observed in the MKN-45 tumors. Consistent with a larger degree of expansion for single CAR T compared with dual CAR T cells, IFNγ and perforin were higher in blood collected from UBS54 mice (**Fig. 6H**).

The superior antitumor efficacy of dual CAR T cells was also observed in the heterogeneous SNU-638 tumor model, which was seeded with 90% EpCAM$^+$ and 10% EpCAM$^-$ cells (**Fig. 7A**). The SNU-638 tumor model had high surface expression of ICAM-1, as opposed to little basal ICAM-1 expression in the MKN-45 tumor model. Similar to the activity against MKN-45 heterogenous tumor (**Fig. 6B–D**), UBS54 CAR T cells retained partial killing of SNU-638 tumors up to 2 weeks after infusion, which then gradually lost the activity against relapsing tumors (**Fig. 7B**). A significant treatment effect was seen only with the dual CAR T cells (**Fig. 7B–D**). Both flow cytometry and IHC analysis showed that relapsing or resistant SNU-638 tumors harvested 5 to 10 weeks after treatment had complete loss of EpCAM expression after single or dual CAR T-cell treatments, indicating these tumors consisted mainly of EpCAM$^-$ SNU-638 cells (**Fig. 7E** and **F**). At the same time, we found higher abundance of T cells in EpCAM$^-$ tumors of dual CAR T cell–treated mice compared with T cells in UBS54 single CAR T cell–treated tumors (**Fig. 7F**). Despite a significantly higher activity of dual CAR T cells over single UBS54 CAR T cells against heterogenous SNU-638 tumors, the low-affinity F292A CAR alone was likely to be insufficient to eliminate the remaining SNU-638 tumors that mainly contained EpCAM$^-$ICAM-1$^+$ cells.

Further reduction of UBS54 CAR affinity may be necessary to avoid on-target off-tumor toxicity

On-target off-tumor reactivity with antigens expressed on normal tissues remains a major safety concern of CAR T cells. Similar to the approach used to test the selectivity of affinity-tuned ICAM-1 CAR T cells against ICAM-1–high tumors in our previous studies (39), we examined cytotoxicity of EpCAM CAR T cells against the primary epithelial cells isolated from human colon, kidney, and liver (Supplementary Fig. S5A). EpCAM expression in these primary cells was intermediate to high, presumably due to enrichment for EpCAM expression by magnetic-activated cell sorting. We used label- and radioisotope-free, impedance-based assays to estimate cells death and found that all three primary EpCAM$^+$ epithelial cells were lysed by UBS54 CAR T cells, similar to the rate of lysis of SNU-638 and HT-29 cells (Supplementary Fig. S5A).

To further examine selectivity of UBS54 CAR T cells toward tumors with higher expression of EpCAM, we used bilateral SNU-638 and SW-1990 tumor models in NSG mice (Supplementary Fig. S5B–D). SW-1990 cell line was chosen for its intermediate EpCAM expression and concordant higher resistance to EpCAM CAR T cells *in vitro* (**Fig.1D**; Supplementary Fig. S2A). In untreated or unrelated CAR T cell (BCMA-specific) cohorts, both SNU-638 and SW-1990 tumors grew comparably. In comparison, UBS54 CAR T cells rapidly eliminated SNU-638 tumors by 2 weeks after treatment, consistent with UBS54 CAR T-cell activity against single site SNU-638 tumors (**Fig. 5B–D**). Despite lower EpCAM expression and higher resistance to UBS54 CAR T cells *in vitro*, SW-1990 tumors were eliminated at a similar rate to SNU-638 by UBS54 CAR T cells.

Discussion

CAR T cells face several unique challenges in solid tumors, including inherent tumor heterogeneity, on-target off-tumor toxicities, and an immunosuppressive tumor microenvironment (40–42). Antigen escape has been recognized as one of the dominant mechanisms of tumor relapse following remission induced by anti-CD19 CAR T cells, and is likely to represent an even greater obstacle in the setting of solid tumors (13). In this study, we aimed to overcome antigen escape by complementing a single CAR against primary antigen with an ICAM-1–targeting CAR using bispecific CAR T cells. Our studies demonstrate that the combined activity of EpCAM-specific and ICAM-1–specific dual CARs significantly enhances the clearance of homogeneous, as well as heterogeneous, tumors and reduces the occurrence of tumor relapse.

We selected ICAM-1 as a complementary target based on our previous experience with CAR T cells targeting this antigen, and because ICAM-1 is an inducible inflammatory molecule that is less likely to undergo downregulation or mutation as do other genetically unstable tumor markers. Although ICAM-1 CAR T cells induce durable CR in systemic anaplastic thyroid cancer models (27, 28), its therapeutic efficacy against gastric tumors appears to be more limited (34). However, in gastric tumor models with homogeneous or heterogeneous EpCAM expression, we demonstrate the significant benefits of combining an ICAM-1–targeting CAR (F292A) with an EpCAM-targeting CAR (UBS54). Our bicistronic design of CARs incorporated two CARs independently encoding CD28 and 41BB costimulatory domains, whereas a single costimulatory domain was used for single CAR T cells (either CD28 or 41BB). Although the superior activity of dual CAR T cells to single EpCAM CAR T cells against EpCAM heterogenous tumors may be anticipated, dual CAR T cells were superior against EpCAM homogeneous tumors. We suspect

Published OnlineFirst August 2, 2021; DOI: 10.1158/2326-6066.CIR-21-0062

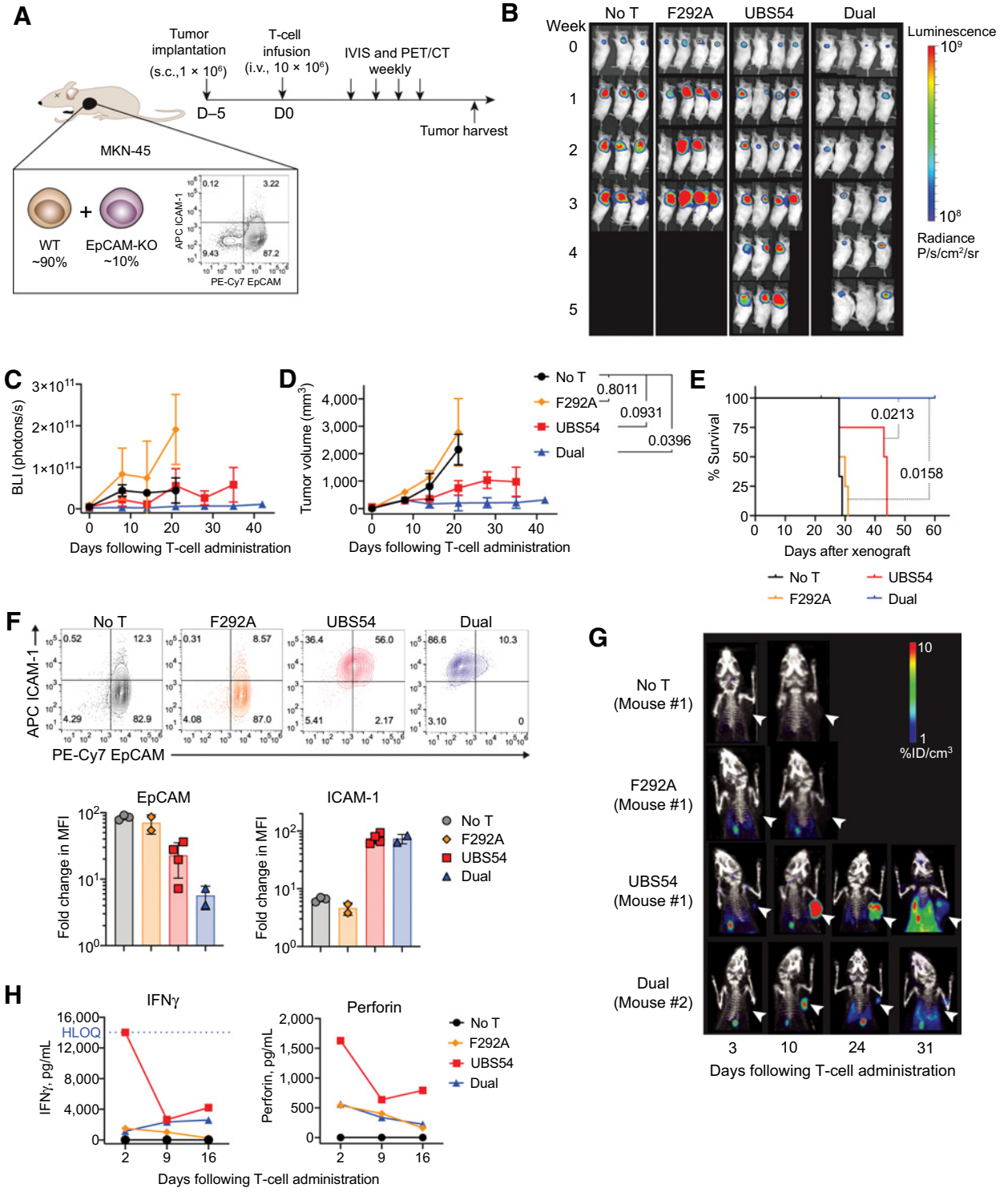

Figure 6.

EpCAM–ICAM-1 dual CAR T cells show enhanced antitumor activity in a heterogeneous MKN-45 tumor model. **A,** Schematic of the heterogeneous MKN-45 tumor model. NSG mice were subcutaneously implanted with a heterogeneous population of MKN-45 cells (90% wild-type, 10% EpCAM-negative, 1×10^6 cells/mouse), and 5 days later received F292A, UBS54, or dual CAR T cells (10×10^6 cells/mouse) via tail vein injection. KO, knockout; WT, wild-type. **B,** Bioluminescence images showing mixed tumor growth over time ($n = 3$–4). **C,** Total-body BLI shown as average values (mean ± SD). **D,** Tumor volume measurements over time (mean ± SD, two-way ANOVA with Tukey multiple comparisons test). **E,** Survival analysis using log-rank (Mantel–Cox) test ($n = 3$–4). **F,** Changes in EpCAM and ICAM-1 cell-surface expression in tumor cells 2 to 8 weeks following CAR T-cell treatment (mean ± SD, $n = 2$–4). **G,** Longitudinal PET/CT images showing ^{18}F-NOTAOCT uptake in CAR T cells. Subcutaneous tumors are indicated by white arrowheads. **H,** Serum IFNγ and perforin measured at 2, 9, and 16 days after T-cell administration. HLOQ, higher limit of quantification.

Published OnlineFirst August 2, 2021; DOI: 10.1158/2326-6066.CIR-21-0062

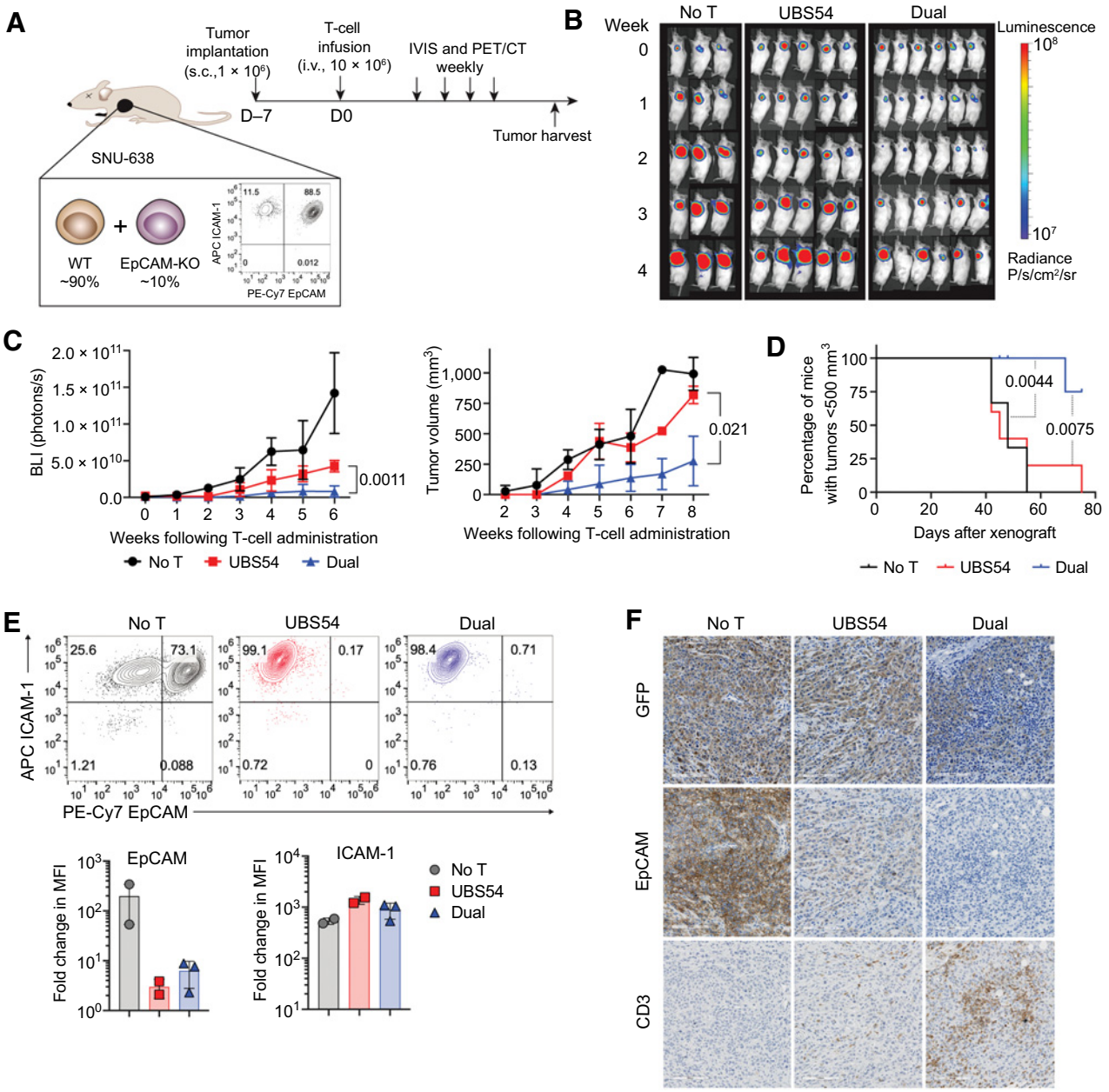

Figure 7.

EpCAM–ICAM-1 dual CAR T mediates longer lasting remission in a heterogeneous SNU-638 tumor model. **A,** Schematic of the heterogeneous SNU-638 tumor model. NSG mice were subcutaneously implanted with a heterogeneous population of SNU-638 cells (90% wild-type, 10% EpCAM-negative, 1×10^6 cells/mouse) and treated 7 days later with UBS54 or dual CAR T cells (10×10^6 cells/mouse) via tail vein injection. KO, knockout; WT, wild-type. **B,** Bioluminescence images showing mixed tumor growth after receiving no treatment (No T; $n = 3$) or treatment with UBS54 ($n = 5$) or dual ($n = 6$) CAR T cells. **C,** Tumor growth shown as average values of total-body BLI or tumor volume, respectively (mean ± SD, $n = 3$–6). *P* values determined by two-way ANOVA with Tukey multiple comparisons test. **D,** Percentage of mice bearing tumors <500 mm^3 ($n = 3$–6). *P* values determined by log-rank (Mantel–Cox) test. **E,** Changes in EpCAM and ICAM-1 cell-surface expression in tumor cells 5 to 10 weeks following CAR T-cell treatment (mean ± SD, $n = 2$–3). **F,** IHC images of GFP, EpCAM, and CD3 (T cells) staining on formalin-fixed, paraffin-embedded tumor sections from untreated mice or mice treated with UBS54 or dual CAR T cells (20× magnification; scale bar, 100 μm). Tumor samples were obtained at 5 weeks following T-cell administration.

that the complementary and additive costimulatory signals through both CD28 and 41BB could be a contributing factor to the greater antitumor response of dual CAR T cells when CARs are engaged with two antigens. Investigation into the antigen profiles of dissociated tumor cells revealed significantly upregulated ICAM-1 in tumors following treatment with CAR T cells, rendering tumor cells more susceptible to dual CAR T cells that additionally target ICAM-1. In particular, although ICAM-1 expression was absent or very low in the MKN-45 tumor model at the time of treatment, ICAM-1 was substantially induced through the proinflammatory cytokines secreted by

Published OnlineFirst August 2, 2021; DOI: 10.1158/2326-6066.CIR-21-0062

CAR T cells upon EpCAM CAR engagement with $EpCAM^+$ tumor cells. In addition to the elevated ICAM-1 expression in many carcinomas (22, 43, 44), including gastric, pancreatic, thyroid, and breast cancers, the inducible nature of ICAM-1 further supports the choice of ICAM-1 as a promising complementary target for the development of multispecific targeted therapies.

In the heterogeneous tumor models, we found a diminished or complete loss of cell-surface EpCAM following treatment with UBS54 or dual CAR T cells. This appears to be the result of selection for preexisting $EpCAM^-$ clones within the heterogeneous population, underscoring tumor heterogeneity as one mechanism of tumor resistance in this model. In addition to preexisting antigen-negative clones, tumor cells can also escape CAR T-cell therapy by losing cell-surface expression of the CAR-targeted antigen after treatment. A proportion of CD19 CAR-resistant tumors involve the enrichment of alternatively spliced CD19 isoforms that lack extracellular epitopes targeted by current CD19-based immunotherapies (9), as well as lineage switching to other hematopoietic lineages (45). However, in the homogeneous EpCAM-expressing tumor models, EpCAM downregulation did not occur in relapsing or resistant tumors. This antigen-positive resistance may involve T-cell dysfunction caused by immune suppression by tumors, judging from retention of EpCAM-high tumors despite infiltration and persistence of UBS54 CAR T cells within tumors. Several approaches have been explored to overcome inhibitory mediators present in the tumor microenvironment, for instance, combination therapy with PD1/PD-L1 checkpoint inhibitors (46, 47), disruption of PD-1/PD-L1 and CTLA-4 pathways (48, 49), deletion of the TGFβ receptor II to suppress regulatory T-cell conversion (50), as well as armoring CAR T cells to deliver stimulatory cytokines (e.g., IL12, IL15, and IL18; refs. 51–53). Therefore, combining dual CARs with these approaches could further enhance T-cell functionality and reduce immune escape.

One major shortcoming of our strategy is that targeting multiple solid tumor antigens could elevate the concerns of on-target off-tumor side effects. The use of affinity-tuned CARs could potentially address this concern and improve the discrimination of tumors from nonmalignant tissues that basally express the same antigens. Although possessing close to micromolar affinity and some selectivity toward cell lines with high EpCAM expression, UBS54 CAR T cells also eliminated primary human epithelial cells. Whether or not the *in vitro* assays using isolated primary cells reflect the *in vivo* CAR T toxicity, particular caution for EpCAM targeting is warranted given various dose-limiting toxicities (DLT) reported in clinical trials with EpCAM-based targeted therapies. High-affinity EpCAM mAbs (3622W94 and ING1) and EpCAM×CD3 T-cell engager solitomab (MT110, AMG 110) have shown off-tumor toxicities (54, 55) and other DLTs, precluding dose escalation to potential therapeutic levels (56). We are currently evaluating EpCAM CAR T cells with lower affinities to limit cell killing to $EpCAM^+$ tumor cells while sparing normal cells with basal EpCAM expression. Multiple clinical trials of EpCAM-specific CAR T cells have already been initiated and will provide more information about the efficacy and safety of targeting EpCAM with CAR T cells (NCT02915445, NCT03013712, and NCT04151186).

As a whole, our study provides proof-of-principle evidence for the superior activity of dual CAR against heterogenous tumors. Upon encountering either $EpCAM^+ICAM\text{-}1^-$, $EpCAM^-ICAM\text{-}1^+$, or $EpCAM^+ICAM\text{-}1^+$ target cells, dual CAR T cells secret pro-inflammatory cytokines in the microenvironment, which further upregulate ICAM-1 in tumor cells through IFNγ and TNFα secretion. $EpCAM^-ICAM\text{-}1^+$ cells that can escape UBS54 single CARs can be recognized and eradicated by dual CARs through ICAM-1 targeting, thereby preventing EpCAM-negative or EpCAM-low relapses (Supplementary Fig. S6). Even in $EpCAM^+ICAM\text{-}1^+$ tumors, additional targeting of ICAM-1 elevates CAR activity against EpCAM, resulting in more durable tumor remission. Given that ICAM-1 can be induced upon CAR T-cell localization and activation, and thus become targetable, our dual CAR design could augment eradication of tumors that are ICAM-1 low or negative at the time of diagnosis. The incorporation of ICAM-1 targeting may thus offer a broadly applicable strategy to boost the antitumor activity of CARs directed against other tumor antigens.

Authors' Disclosures

E. von Hofe reports other support from AffyImmune Therapeutics, Inc. during the conduct of the study, as well as other support from AffyImmune Therapeutics, Inc. outside the submitted work. M.M. Jin reports grants from AffyImmune Therapeutics, Inc. during the conduct of the study, as well as grants from AffyImmune Therapeutics, Inc. outside the submitted work. No disclosures were reported by the other authors.

Authors' Contributions

Y. Yang: Conceptualization, data curation, software, formal analysis, validation, investigation, methodology, writing–original draft, writing–review and editing. **J.E. McCloskey:** Data curation, software, formal analysis, investigation, writing–review and editing. **H. Yang:** Conceptualization, data curation, software, formal analysis, investigation. **J. Puc:** Data curation, software, formal analysis, methodology. **Y. Alcaina:** Data curation, software, formal analysis, investigation. **Y. Vedvyas:** Data curation, formal analysis, investigation, methodology. **A.A. Gomez Gallegos:** Conceptualization, investigation, methodology. **E. Ortiz-Sánchez** Conceptualization, resources. **E. de Stanchina:** Resources, methodology, writing–review and editing. **I.M. Min:** Resources, supervision, funding acquisition, project administration, writing–review and editing. **E. von Hofe:** Resources, supervision, funding acquisition, project administration, writing–review and editing. **M.M. Jin:** Conceptualization, resources, supervision, funding acquisition, project administration, writing–review and editing.

Acknowledgments

This work was supported by NIH grants R01-CA217059-04, R01-CA254035-01A1, and U54OD020355-01; a sponsored research grant (AffyImmune Therapeutics, Inc.); and an institutional grant (MI3, Weill Cornell Medicine). The authors acknowledge the support of the Department of Pathology and Laboratory Medicine, Citigroup Biomedical Imaging Center at Weill Cornell Medicine, and Molecular Cytology Core Facility at Memorial Sloan Kettering Cancer Center.

The costs of publication of this article were defrayed in part by the payment of page charges. This article must therefore be hereby marked *advertisement* in accordance with 18 U.S.C. Section 1734 solely to indicate this fact.

Received January 25, 2021; revised April 26, 2021; accepted July 29, 2021; published first July 30, 2021.

References

1. Jackson HJ, Rafiq S, Brentjens RJ. Driving CAR T-cells forward. Nat Rev Clin Oncol 2016;13:370–83.
2. Sadelain M, Rivière I, Riddell S. Therapeutic T cell engineering. Nature 2017;545:423–31.

3. June CH, Sadelain M. Chimeric antigen receptor therapy. N Engl J Med 2018;379:64–73.
4. Maude SL, Frey N, Shaw PA, Aplenc R, Barrett DM, Bunin NJ, et al. Chimeric antigen receptor T cells for sustained remissions in leukemia. N Engl J Med 2014;371:1507–17.
5. Brudno JN, Kochenderfer JN. Chimeric antigen receptor T-cell therapies for lymphoma. Nat Rev Clin Oncol 2018;15:31–46.
6. Brudno JN, Maric I, Hartman SD, Rose JJ, Wang M, Lam N, et al. T cells genetically modified to express an anti–B-cell maturation antigen chimeric antigen receptor cause remissions of poor-prognosis relapsed multiple myeloma. J Clin Oncol 2018;36:2267–80.
7. Cohen AD, Garfall AL, Stadtmauer EA, Melenhorst JJ, Lacey SF, Lancaster E, et al. B cell maturation antigen-specific CAR T cells are clinically active in multiple myeloma. J Clin Invest 2019;129:2210–21.
8. Park JH, Rivière I, Gonen M, Wang X, Sénéchal B, Curran KJ, et al. Long-term follow-up of CD19 CAR therapy in acute lymphoblastic leukemia. N Engl J Med 2018;378:449–59.
9. Sotillo E, Barrett DM, Black KL, Bagashev A, Oldridge D, Wu G, et al. Convergence of acquired mutations and alternative splicing of CD19 enables resistance to CART-19 immunotherapy. Cancer Discov 2015;5:1282–95.
10. Gardner R, Wu D, Cherian S, Fang M, Hanafi LA, Finney O, et al. Acquisition of a CD19-negative myeloid phenotype allows immune escape of MLL-rearranged B-ALL from CD19 CAR-T-cell therapy. Blood 2016;127:2406–10.
11. Fry TJ, Shah NN, Orentas RJ, Stetler-Stevenson M, Yuan CM, Ramakrishna S, et al. CD22-targeted CAR T cells induce remission in B-ALL that is naive or resistant to CD19-targeted CAR immunotherapy. Nat Med 2018;24:20–8.
12. Burrell RA, McGranahan N, Bartek J, Swanton C. The causes and consequences of genetic heterogeneity in cancer evolution. Nature 2013;501:338–45.
13. Majzner RG, Mackall CL. Tumor antigen escape from CAR T-cell therapy. Cancer Discov 2018;8:1219–26.
14. O'Rourke DM, Nasrallah MP, Desai A, Melenhorst JJ, Mansfield K, Morrissette JJD, et al. A single dose of peripherally infused EGFRvIII-directed CAR T cells mediates antigen loss and induces adaptive resistance in patients with recurrent glioblastoma. Sci Transl Med 2017;9:eaaa0984.
15. Shah NN, Johnson BD, Schneider D, Zhu F, Szabo A, Keever-Taylor CA, et al. Bispecific anti-CD20, anti-CD19 CAR T cells for relapsed B cell malignancies: a phase 1 dose escalation and expansion trial. Nat Med 2020;26:1569–75.
16. Ruella M, Barrett DM, Kenderian SS, Shestova O, Hofmann TJ, Perazzelli J, et al. Dual CD19 and CD123 targeting prevents antigen-loss relapses after CD19-directed immunotherapies. J Clin Invest 2016;126:3814–26.
17. Hegde M, Mukherjee M, Grada Z, Pignata A, Landi D, Navai SA, et al. Tandem CAR T cells targeting HER2 and IL13Rα2 mitigate tumor antigen escape. J Clin Invest 2016;126:3036–52.
18. Rothlein R, Dustin ML, Marlin SD, Springer TA. A human intercellular adhesion molecule (ICAM-1) distinct from LFA-1. J Immunol 1986;137:1270–4.
19. Dustin ML, Rothlein R, Bhan AK, Dinarello CA, Springer TA. Induction by IL 1 and interferon-gamma: tissue distribution, biochemistry, and function of a natural adherence molecule (ICAM-1). J Immunol 1986;137:245–54.
20. Park S, Kang S, Chen X, Kim EJ, Kim J, Kim N, et al. Tumor suppression via paclitaxel-loaded drug carriers that target inflammation marker upregulated in tumor vasculature and macrophages. Biomaterials 2013;34:598–605.
21. Sherbenou DW, Su Y, Behrens CR, Aftab BT, Perez de Acha O, Murnane M, et al. Potent activity of an anti-ICAM1 antibody–drug conjugate against multiple myeloma. Clin Cancer Res 2020;26:6028–38.
22. Guo P, Huang J, Wang L, Jia D, Yang J, Dillon DA, et al. ICAM-1 as a molecular target for triple negative breast cancer. Proc Natl Acad Sci U.S.A 2014;111:14710–5.
23. Kotteas EA, Boulas P, Gkiozos I, Tsagkouli S, Tsoukalas G, Syrigos KN. The intercellular cell adhesion molecule-1 (ICAM-1) in lung cancer: implications for disease progression and prognosis. Anticancer Res 2014;34:4665–72.
24. Damiano JS, Cress AE, Hazlehurst LA, Shtil AA, Dalton WS. Cell adhesion mediated drug resistance (CAM-DR): role of integrins and resistance to apoptosis in human myeloma cell lines. Blood 1999;93:1658–67.
25. Hansson M, Gimsing P, Badros A, Niskanen TM, Nahi H, Offner F, et al. A phase I dose-escalation study of antibody BI-505 in relapsed/refractory multiple myeloma. Clin Cancer Res 2015;21:2730–6.
26. Haug CE, Colvin RB, Delmonico FL, Auchincloss H Jr, Tolkoff-Rubin N, Preffer FI, et al. A phase I trial of immunosuppression with anti-ICAM-1 (CD54) mAb in renal allograft recipients. Transplantation 1993;55:766–72.
27. Park S, Shevlin E, Vedvyas Y, Zaman M, Park S, Hsu YMS, et al. Micromolar affinity CAR T cells to ICAM-1 achieves rapid tumor elimination while avoiding systemic toxicity. Sci Rep 2017;7:14366.
28. Min IM, Shevlin E, Vedvyas Y, Zaman M, Wyrwas B, Scognamiglio T, et al. CAR T therapy targeting ICAM-1 eliminates advanced human thyroid tumors. Clin Cancer Res 2017;23:7569–83.
29. Huls GA, Heijnen IAFM, Cuomo ME, Koningsberger JC, Wiegman L, Boel E, et al. A recombinant, fully human monoclonal antibody with antitumor activity constructed from phage-displayed antibody fragments. Nat Biotechnol 1999;17:276–81.
30. Went PTH, Lugli A, Meier S, Bundi M, Mirlacher M, Sauter G, et al. Frequent EpCam protein expression in human carcinomas. Hum Pathol 2004;35:122–8.
31. Oden F, Marino SF, Brand J, Scheu S, Kriegel C, Olal D, et al. Potent anti-tumor response by targeting B cell maturation antigen (BCMA) in a mouse model of multiple myeloma. Mol Oncol 2015;9:1348–58.
32. Mattar M, McCarthy CR, Kulick AR, Qeriqi B, Guzman S, de Stanchina E. Establishing and maintaining an extensive library of patient-derived xenograft models. Front Oncol 2018;8:19.
33. Ku JL, Park JG. Biology of SNU cell lines. Cancer Res Treat 2005;37:1–19.
34. Jung M, Yang Y, McCloskey JE, Zaman M, Vedvyas Y, Zhang X, et al. Chimeric antigen receptor T Cell therapy targeting ICAM-1 in gastric cancer. Mol Ther Oncolytics 2020;18:587–601.
35. Nam HJ, Ching KA, Kan J, Kim HP, Han SW, Im SA, et al. Evaluation of the antitumor effects and mechanisms of PF00299804, a pan-HER inhibitor, alone or in combination with chemotherapy or targeted agents in gastric cancer. Mol Cancer Ther 2012;11:439–51.
36. Motoyama T, Hojo H, Watanabe H. Comparison of seven cell lines derived from human gastric carcinomas. Acta Pathol Jpn 1986;36:65–83.
37. Vedvyas Y, Shevlin E, Zaman M, Min IM, Amor-Coarasa A, Park S, et al. Longitudinal PET imaging demonstrates biphasic CAR T cell responses in survivors. JCI Insight 2016;1:e90064.
38. Upadhyay R, Boiarsky JA, Pantsulaia G, Svensson-Arvelund J, Lin MJ, Wroblewska A, et al. A critical role for Fas-mediated off-target tumor killing in T-cell immunotherapy. Cancer Discov 2021;11:599–613.
39. Vedvyas Y, McCloskey JE, Yang Y, Min IM, Fahey TJ, Zarnegar R, et al. Manufacturing and preclinical validation of CAR T cells targeting ICAM-1 for advanced thyroid cancer therapy. Sci Rep 2019;9:10634.
40. Dunn GP, Old LJ, Schreiber RD. The three Es of cancer immunoediting. Annu Rev Immunol 2004;22:329–60.
41. Shah NN, Fry TJ. Mechanisms of resistance to CAR T cell therapy. Nat Rev Clin Oncol 2019;16:372–85.
42. Rafiq S, Hackett CS, Brentjens RJ. Engineering strategies to overcome the current roadblocks in CAR T cell therapy. Nat Rev Clin Oncol 2020;17:147–67.
43. Jung WC, Jang YJ, Kim JH, Park SS, Park SH, Kim SJ, et al. Expression of intercellular adhesion molecule-1 and e-selectin in gastric cancer and their clinical significance. J Gastric Cancer 2012;12:140–8.
44. Huang J, Agoston AT, Guo P, Moses MA. A rationally designed ICAM1 antibody drug conjugate for pancreatic cancer. Adv Sci 2020;7:2002852.
45. Jacoby E, Nguyen SM, Fountaine TJ, Welp K, Gryder B, Qin H, et al. CD19 CAR immune pressure induces B-precursor acute lymphoblastic leukaemia lineage switch exposing inherent leukaemic plasticity. Nat Commun 2016;7:12320.
46. Gray KD, McCloskey JE, Vedvyas Y, Kalloo OR, Eshaky SE, Yang Y, et al. PD1 blockade enhances ICAM1-Directed CAR T therapeutic efficacy in advanced thyroid cancer. Clin Cancer Res 2020;26:6003–16.
47. Chong EA, Melenhorst JJ, Svoboda J, Nasta SD, Landsburg DJ, Mato AR, et al. Phase I/II study of pembrolizumab for progressive diffuse large B cell lymphoma after anti-CD19 directed chimeric antigen receptor modified T cell therapy. Blood 2017;130:4121.
48. Cherkassky L, Morello A, Villena-Vargas J, Feng Y, Dimitrov DS, Jones DR, et al. Human CAR T cells with cell-intrinsic PD-1 checkpoint blockade resist tumor-mediated inhibition. J Clin Invest 2016;126:3130–44.
49. Condomines M, Arnason J, Benjamin R, Gunset G, Plotkin J, Sadelain M. Tumor-targeted human T cells expressing CD28-based chimeric antigen receptors circumvent CTLA-4 inhibition. PLoS One 2015;10:e0130518.
50. Tang N, Cheng C, Zhang X, Qiao M, Li N, Mu W, et al. TGF-β inhibition via CRISPR promotes the long-term efficacy of CAR T cells against solid tumors. JCI Insight 2020;5:e133977.
51. Chinnasamy D, Yu Z, Kerkar SP, Zhang L, Morgan RA, Restifo NP, et al. Local delivery of Interleukin-12 using T cells targeting VEGF receptor-2

Published OnlineFirst August 2, 2021; DOI: 10.1158/2326-6066.CIR-21-0062

eradicates multiple vascularized tumors in mice. Clin Cancer Res 2012;18:1672–83.
52. Krenciute G, Prinzing BL, Yi Z, Wu M-F, Liu H, Dotti G, et al. Transgenic expression of IL15 improves antiglioma activity of IL13Rα2-CAR T cells but results in antigen loss variants. Cancer Immunol Res 2017;5:571–81.
53. Hu B, Ren J, Luo Y, Keith B, Young RM, Scholler J, et al. Augmentation of antitumor immunity by human and mouse CAR T cells secreting IL-18. Cell Rep 2017;20:3025–33.
54. de Bono JS, Tolcher AW, Forero A, Vanhove GFA, Takimoto C, Bauer RJ, et al. ING-1, a monoclonal antibody targeting Ep-CAM in patients with advanced adenocarcinomas. Clin Cancer Res 2004;10:7555–65.
55. Münz M, Murr A, Kvesic M, Rau D, Mangold S, Pflanz S, et al. Side-by-side analysis of five clinically tested anti-EpCAM monoclonal antibodies. Cancer Cell Int 2010;10:44.
56. Kebenko M, Goebeler ME, Wolf M, Hasenburg A, Seggewiss-Bernhardt R, Ritter B, et al. A multicenter phase 1 study of solitomab (MT110, AMG 110), a bispecific EpCAM/CD3 T-cell engager (BiTE®) antibody construct, in patients with refractory solid tumors. Oncoimmunology 2018;7:e1450710.

AACR American Association for Cancer Research

Cancer Immunology Research

Bispecific CAR T Cells against EpCAM and Inducible ICAM-1 Overcome Antigen Heterogeneity and Generate Superior Antitumor Responses

Yanping Yang, Jaclyn E. McCloskey, Huan Yang, et al.

Cancer Immunol Res Published OnlineFirst August 2, 2021.